



Review

Metals in Imaging of Alzheimer's Disease

Olga Krasnovskaya ^{1,2,*} , Daniil Spector ^{1,2,*} , Alexander Zlobin ¹, Kirill Pavlov ¹,
Peter Gorelkin ^{1,2} , Alexander Erofeev ^{1,2}, Elena Beloglazkina ¹ and Alexander Majouga ^{1,2,3}

¹ Chemistry Department, Lomonosov Moscow State University, Leninskie Gory 1,3, 119991 Moscow, Russia; zlobinabchem@gmail.com (A.Z.); kirill.pavlov2011@mail.ru (K.P.); peter.gorelkin@gmail.com (P.G.); Erofeev@polly.phys.msu.ru (A.E.); beloglazki@mail.ru (E.B.); alexander.majouga@gmail.com (A.M.)

² Department of Materials Science of Semiconductors and Dielectrics, National University of Science and Technology (MISIS), Leninskiy Prospekt 4, 101000 Moscow, Russia

³ Mendeleev University of Chemical Technology of Russia, Miusskaya Ploshchad' 9, 125047 Moscow, Russia

* Correspondence: krasnovskayao@gmail.com (O.K.); danspector@yandex.ru (D.S.)

Received: 10 November 2020; Accepted: 28 November 2020; Published: 2 December 2020



Abstract: One of the hallmarks of Alzheimer's disease (AD) is the deposition of amyloid plaques in the brain parenchyma, which occurs 7–15 years before the onset of cognitive symptoms of the pathology. Timely diagnostics of amyloid formations allows identifying AD at an early stage and initiating inhibitor therapy, delaying the progression of the disease. However, clinically used radiopharmaceuticals based on ¹¹C and ¹⁸F are synchrotron-dependent and short-lived. The design of new metal-containing radiopharmaceuticals for AD visualization is of interest. The development of coordination compounds capable of effectively crossing the blood-brain barrier (BBB) requires careful selection of a ligand moiety, a metal chelating scaffold, and a metal cation, defining the method of supposed A β visualization. In this review, we have summarized metal-containing drugs for positron emission tomography (PET), magnetic resonance imaging (MRI), and single-photon emission computed tomography (SPECT) imaging of Alzheimer's disease. The obtained data allow assessing the structure-ability to cross the BBB ratio.

Keywords: Alzheimer disease; amyloid; PET; SPECT; MRI

1. Introduction

Alzheimer's disease is the most common form of neurodegenerative disease. This pathology is characterized by the presence of extracellular amyloid plaques and intracellular neurofibrillary tangles (NFTs) in the brain [1]. One of the hallmarks is the extracellular amyloid plaques in aggregated forms of a peptide called amyloid- β (A β), appearing years before the onset of symptoms [2–5].

Timely diagnostic imaging plays an important role in managing AD. Several positron emission tomography (PET) imaging agents have been developed that bind to different amyloids, such as 2-(1,1-dicyanopropen-2-yl)-6-(2-[¹⁸F]-fluoroethyl)-methylamino-naphthalene [¹⁸F]FDDNP, [¹¹C]Pittsburgh Compound-B (PiB), [¹⁸F]Florbetapir, [¹⁸F]Florbetaben, and [¹⁸F]Flutemetamol, allow obtaining semiquantitative information about amyloid deposition in patients, which allows presaging the development of clinical symptoms of AD 7–15 years before their occurrence [6–10] (Figure 1). But using these drugs requires an expensive laborious synthesis with confirmation of radio purity at each stage. The short half-lives of the currently used radionuclides ¹¹C (20.4 min) and ¹⁸F (109.8 min) may also limit the widespread use of these imaging agents [11,12].

Although metal cations such as Cu(II), Zn(II), and Fe(III) proved to coordinate undesirably with histidine residues at the N-terminus of A β , promoting A β aggregation and stabilization of A β oligomers [13], an increased accumulation of these metals in A β -amyloids raises the possibility of

designing Cu(II)-, Zn(II)-, and Fe(III)-based metal complexes for the diagnosis and theranostics of AD. AD diagnostic agents radiolabeled with ^{64}Cu are attractive not only due to the simple and fast introduction of radionuclide at the last stage of non-radioactive synthesis, but also due to the 12.7 h half-life of ^{64}Cu radionuclide, ideal for PET imaging [14].

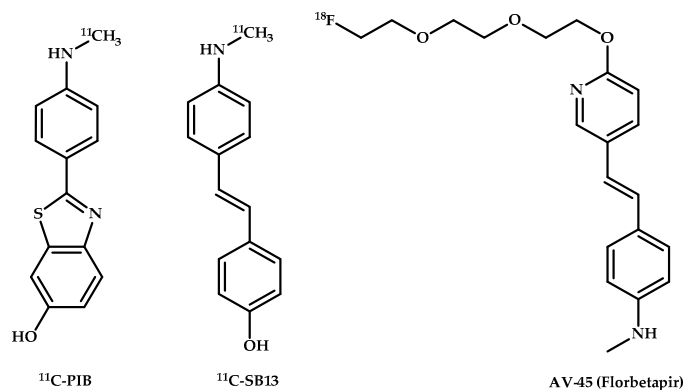


Figure 1. Pittsburgh compound B (PiB), [^{11}C]4-N-Methylamino-4'-hydroxystilbene (SB-13), and Florbetair (AV-45), AD PET imaging agents.

Another promising PET radionuclide is ^{68}Ga . Positron-emitting ^{68}Ga can be obtained from a $^{68}\text{Ge}/^{68}\text{Ga}$ generator, which would allow a cyclotron-independent distribution of PET. The parent nuclide, ^{68}Ge , has a half-life of 271 days, and the generators can provide sufficient quantities of ^{68}Ga for up to one year, resulting in a relatively inexpensive and reliable source of a positron-emitting radionuclide [15,16].

In addition to PET imaging of amyloids, single-photon emission computed tomography (SPECT) and magnetic resonance imaging (MRI) are alternative diagnostic tools for AD visualization, able to overcome the limitations of PET imaging in terms of cost and broad accessibility [17]. The technetium-99m ($^{99\text{m}}\text{Tc}$) radioisotope for SPECT imaging can be cyclotron-independently prepared by a $^{99}\text{Mo}/^{99\text{m}}\text{Tc}$ generator [18]. The MRI imaging allows nonradioactive diagnostics and is also cheaper and faster than PET imaging. The Gd^{3+} PET imaging agents for $\text{A}\beta$ visualization are also of interest [19].

The development of effective diagnostic and therapeutic agents targeting amyloid is not a trivial task. The blood-brain barrier (BBB) is a highly selective, semipermeable barrier, consistent of cerebrovascular endothelial cells, surrounded by extracellular matrix, astrocytes, and pericytes [20], which prevents potential therapeutics from reaching the cerebral target, thus limiting their efficacy [21]. Various approaches to effective brain delivery are developed, such as chemical drug delivery systems [22], e.g., a drug conjugation with dihydropyridine, mannitol, or aromatic substances [23], physical methods, such as focused ultrasound [24] or sonophoresis [25], and biological methods, e.g., drug conjugation with polycationic proteins or amino acids [26].

The complexity of the architecture of the blood-brain barrier, as well as the significant difficulties accompanying the development of drugs capable of overcoming it, prompts the creation of in vitro models of the BBB, such as microfluidic models [27], brain organoids [28], and microvascular systems [29].

The BBB permeability of a compound is related to its lipophilicity, expressed by the water/octanol partition coefficient, $\log P_{\text{oct/water}}$, molecular weight (MW), and plasma pharmacokinetics [30]. Low-MW amphiphilic molecules with $\log P_{\text{oct/water}} \approx 2$ have optimal BBB penetration [31]. Conjugating an $\text{A}\beta$ -affinity moiety, a metal-chelating moiety, and a metal cation in one scaffold is often difficult, and the resulting drugs are often unable to cross the BBB.

Sedgwick et al. summarized metal-based imaging agents for neurodegenerative disease diagnostics [32]. Gomes et al. also summarized an interaction of metal complexes with the $\text{A}\beta$ peptide [33]. Liu et al. reported potential applications of metal-based agents in therapy, diagnosis, and theranosis of AD [34].

In this review, we summarize various solutions in the design of amyloid-affinity drugs capable of effectively crossing the BBB, and different approaches for designing A β -affinity drugs for diagnosing AD. Three summary tables can be conveniently used to evaluate the structure of the ligand and the result of brain penetration by the coordination compound based on it, noting the successful and unsuccessful attempts to create drugs for diagnosing AD. This review will be useful to researchers for developing approaches for designing A β -affinity drugs for both the therapy and diagnostics of AD.

2. Copper Coordination Compounds for PET Imaging of Alzheimer Disease

PET diagnostics is based on registering a pair of gamma quanta resulting from the annihilation of electrons and positrons that arise during the positron-beta decay of a radionuclide. Annihilation of the positron, which remained in the tissue, with one of the electrons of the medium, generates two gamma quanta with the same energy, scattering in opposite directions along one straight line. A set of detectors makes it possible to obtain a three-dimensional reconstruction of the distribution of the radionuclide in the body tissue [35].

The radionuclide ^{64}Cu has a long half-life ($t_{1/2} = 12.7$ h, $\beta^+ = 17\%$, $\beta^- = 39\%$, e-capture decay EC = 43%, $E_{\text{max}} = 0.656$ MeV) and can be considered an ideal PET tracer [36]. Copper-coordination compounds are promising for PET diagnostics of AD because of not only the emission properties but also the increased affinity of amyloids for copper cations, which would further increase the accumulation of copper-containing drugs in the therapeutic target [37].

A standard approach in developing A β PET imaging drugs is a conjugation of an A β -binding benzothiazole, benzofuran, or stilbene scaffold, with a metal-chelating moiety. Thiosemicarbazone derivatives are often used as a metal-chelating agent, based on the diacetylbis(N(4)-methylthiosemicarbazonato Cu-ATSM drug [38].

Lim et al. [39] developed a bis(thiosemicarbazonato)copper(II) complex **1** (all numbers of coordination compounds are bold through all the manuscript) conjugated with a stilbene functional group (Figure 2). A fluorescent assay with thioflavin-T (Th-T) showed a drop in the fluorescence (485 nm) after an addition of coordination compound **1**, meaning a displacement of thioflavin. Also, examination by transmission electron microscopy (TEM) of the structural morphology of the A β fibrils pre-treated with coordination compound **1** showed significant changes in morphology. Epi-fluorescence microscopy of AD human brain sections with E18 antibody revealed a co-localization of the immunostained and epi-fluorescent images. Biodistribution of radiolabeled ^{64}Cu -**1** in wild-type mice and *APP/PS1* transgenic mice (Tg-mice) after intravenous tail vein injection (85 MBq) showed a significantly higher brain uptake in *APP/PS1* Tg-mice compared with their wild type (Table 1).

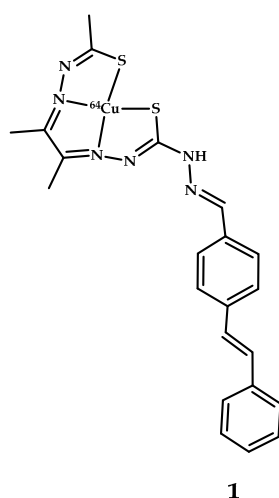


Figure 2. ^{64}Cu (II)-ATSM derivative **1** conjugated with stilbene functional group, designed for A β fibrils visualization.

Table 1. Cu(II)-based coordination compounds for positron emission tomography (PET) imaging of Alzheimer disease.

| Coordination Compound Number | Brain Uptake, ID/g, 2 min Post-Injection, % | Brain _{2min/60min} (*Brain _{2min/30min}) Ratio | Brain Tissue Experiments | A β Binding Moiety | Reference |
|---------------------------------------|--|---|---|------------------------------------|-----------|
| Cu(ATSM)-based coordination compounds | | | | | |
| 1 | 2.5 \pm 0.6 (<i>APP/PS1</i> transgenic mice) 1.7 \pm 0.6 (Wild-type mice) 7 min after injection | - | Epi-fluorescence microscopy of AD human brain sections | Stilbene | [39] |
| 2–4 | 1.11 \pm 0.20 | 2.92 * | Epi-fluorescence microscopy of AD human brain sections | 2-benzothiazole,3,4-styrylpyridine | [40] |
| 5–8 | 1.39 \pm 0.06 1.06 \pm 0.43 0.77 \pm 0.19 1.54 \pm 0.60 | 1.31 * 2.16 * 1.05 * | Elemental composition of AD human brain tissue using LA-ICP-MS | Benzofuran | [41] |
| 9 | - | - | Epi-fluorescence microscopy of AD human brain tissue (ligand) | Stilbene | [42] |
| 10–15 | 2.2 \pm 0.6 1.1 \pm 0.2 | 6.47 5 | Epi-fluorescence microscopy of AD human brain sections | Styrylpyridine | [43] |
| 16–25 | 4.41 \pm 0.23 (23 h Post-injection similar) | - | PET imagine of BALB/c mice | - | [44] |
| Other metal-chelating moieties | | | | | |
| 26, 27 | 0.33 \pm 0.12 0.36 \pm 0.10 | 1.83 2.11 | Fluorescent staining using brain sections from a Tg2576 mice | Benzofuran | [45] |
| 29–33 | 0.37 \pm 0.06 0.17 \pm 0.02 1.33 \pm 0.27 0.49 \pm 0.01 0.61 \pm 0.14 0.75 \pm 0.16 | 2.64 1.30 4.92 2.22 4.69 2.88 | Fluorescent imaging of amyloid plaques in Tg2576 AD mice brain sections | Benzothiazole | [46,47] |
| 34–39 | 0.16 \pm 0.02 0.99 \pm 0.04 | 1.59 4.95 | Fluorescence imaging of amyloid plaques in 5xFAD mice brain sections | Benzothiazole | [48] |

* Brain_{2min/30min} ratio is indicated instead of Brain_{2min/60min} ratio.

The same Donnelly group reported a copper radiopharmaceutical Cu(II)-ATSM with an appended styrylpyridine functional group for A β plaque imaging [40] (Figure 3). Binding of **3** and **4** (coordination compound **2** was quite insoluble) to A β plaques was clearly evident, as demonstrated by epi-fluorescence microscopy. The A β -specific 1E8 antibody was used as a control. The biodistribution of coordination compounds **3** and **4** radiolabeled with ^{64}Cu in wild-type mice after intravenous tail injection (~13 MBq) displayed good brain uptake of coordination compound **4** in 1.1%.

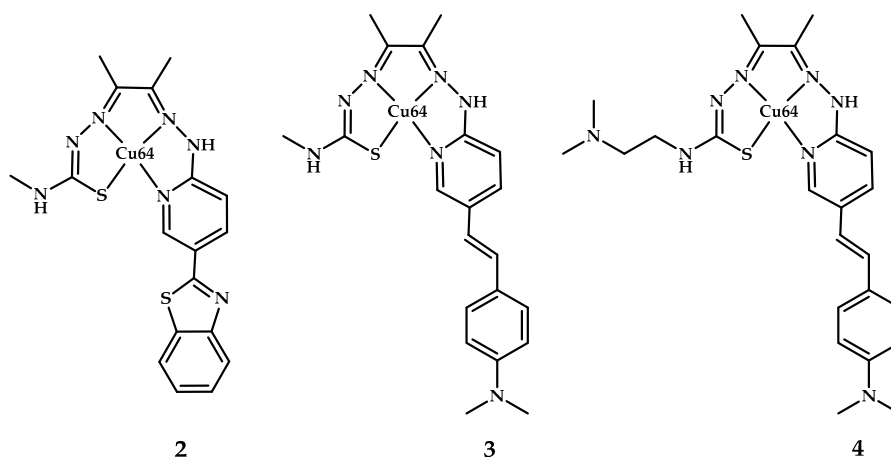


Figure 3. ^{64}Cu (II)-ATSM derivatives conjugated **2–4** with benzothiazole/styrylpyridine functional group, designed for A β fibrils visualization.

In 2019 [41], the Donnelly group reported a synthesis of four hybrid thiosemicarbazonato-benzofuran ligands and their copper complexes (Figure 4). Addition of either **6** or **8** to A β_{1-42} results in dramatic changes in the structural morphology, as identified by the TEM images. The AD human brain tissue samples treated with **8** were analyzed for elemental composition using the laser ablation inductively coupled plasma mass spectrometry (LA-ICP-MS) assay by tracking the change in the ratio $^{65}\text{Cu}/^{63}\text{Cu}$. A sample of nonradioactive isotopically enriched ^{65}Cu -**8** was used to distinguish biologically present copper from the complex. Coordination compound **3** was used as a control. The benzofuran-containing complex ^{65}Cu -**8** appears to bind with improved differentiation compared with the styryl-pyridine-containing complex ^{65}Cu -**3** and potentially offers better sensitivity for amyloid. The complex preferentially binds to areas of the brain enriched with A β plaques, which was confirmed by immunohistochemistry with an aged-match control. The biodistribution of coordination compounds **5–8** radiolabeled with ^{64}Cu in wild-type mice showed the best brain uptake results for coordination compound **8** (1.54% of injected dose (ID)/g at 2 min after injection, dropping to 0.77% ID/g at 30 min).

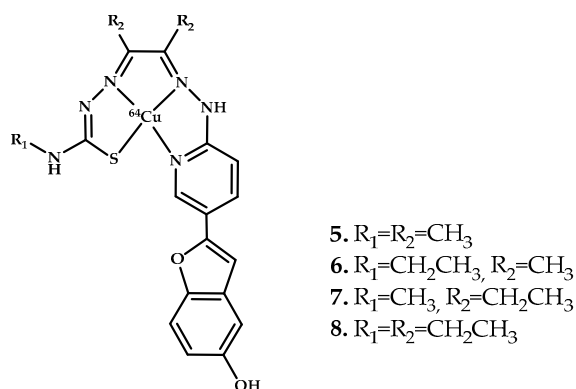


Figure 4. ^{64}Cu (II)-ATSM derivatives **5–8** conjugated with benzofuran functional group, designed for A β fibrils visualization.

McInne [42] incorporated a 4-vinylpyridine functional group to investigate whether the complex **9** binds to A β plaques with an additional pyridyl hydrogen bond acceptor at the expense of the electron-donating dimethylamino and hydroxy groups (Figure 5). Comparing the fluorescence from the **9**-treated AD human brain tissue with (1E8)-treated brain tissue revealed good co-localization.

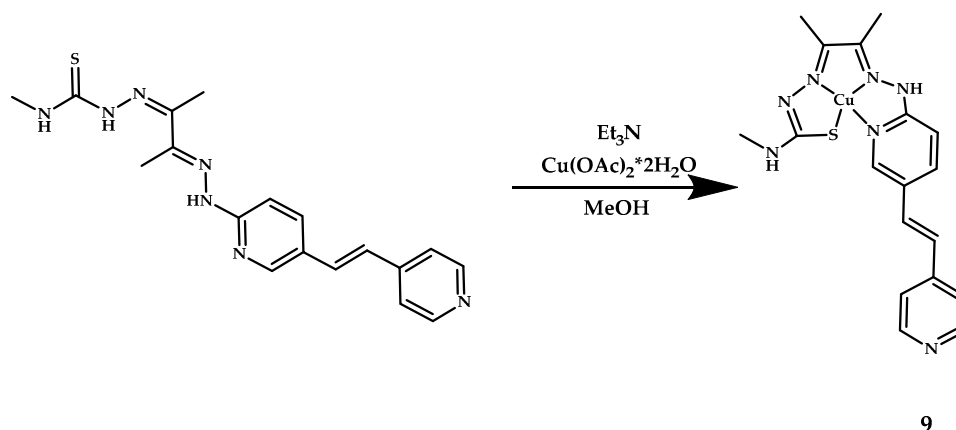


Figure 5. Cu(II)-ATSM derivative conjugated with piridylstilbene functional group **9**, designed for A β fibrils visualization.

This research group recently presented several structural analogues (**10–15**) of coordination compound **3**, where the bis-(thiosemicarbazone) moiety is conjugated to stilbene functional groups [44] (Figure 6). All coordination compounds significantly alter the emission intensity of the ThT/A β conjugate. Compounds **11** and **15** were selected as lead compounds because of the ease of synthesis. The TEM of A β _{1–40} fibrils preincubated with **11** and **15** reveal a dramatic change in fibril morphology. Epi-fluorescence microscopy on human AD brain tissue proved an ability of **11** and **15** to bind amyloid- β plaques, which was also confirmed by A β -specific antibody (1E8) staining. Experiments with wild-type mice showed high brain uptake for both **11** and **15** at 2 min after the injection (2.2% and 1.1%, respectively), followed by rapid removal after 1 h.

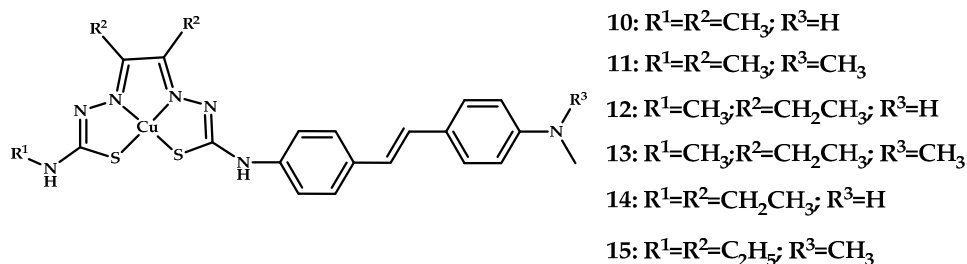


Figure 6. Cu(II)-ATSM derivatives conjugated with stilbene functional groups **10–15**, designed for A β fibrils visualization.

Observing the various design steps of the PET binding agents developed under Donnelly's leadership, we note that they achieved significant improvements in brain uptake (Table 1, lines 3–7).

Paterson et al. [44] developed a series bis(thiosemicarbazones) **16–25** with amine and polyamine functional groups in order to increase the BBB permeability of the complexes (Figure 7). Intracellular uptake of the complexes was measured by inductively coupled plasma mass spectrometry (ICP-MS). Intracellular accumulation decreased in the order **17** > [**19** + 2H]²⁺ > [**21** + H]⁺ > [**23** + H]⁺ > [**25** + 3H]³⁺. Biodistribution studies were performed using small-animal micro-PET imaging. The complexes with a secondary amine, **21**, and a primary amine functional group, **23**, showed little to no radioactivity in the brain. The complex with a pendent secondary amine, **17**, had a relatively high level of brain uptake.

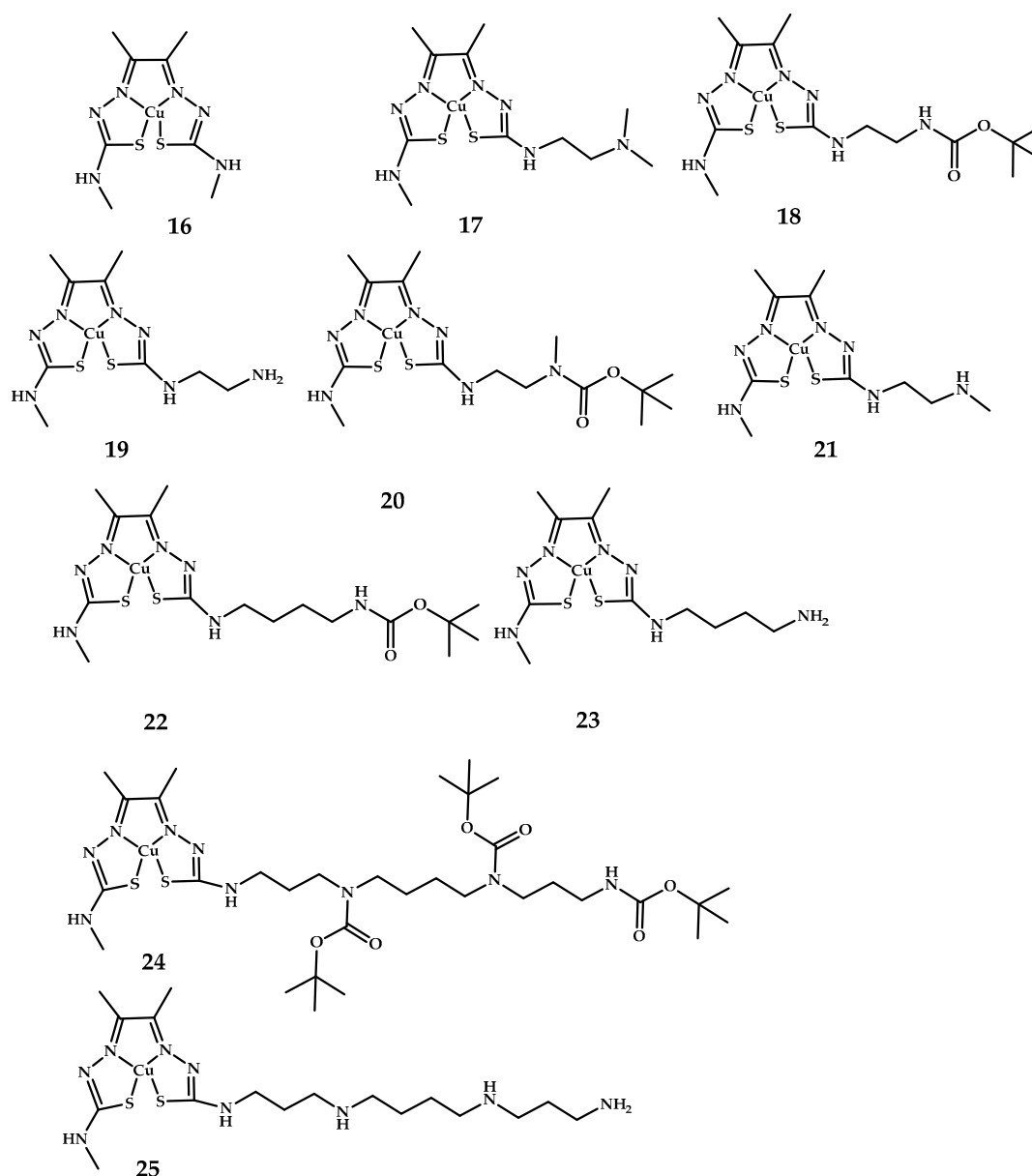


Figure 7. Cu(II)-ATSM derivatives conjugated with polyamines 16–25, designed for A β fibrils visualization.

The authors designed these complexes not as PET imaging agents for amyloids, but as hypoxia-sensitive agents capable of accumulating in malignant tumors. But the impressive results of brain penetration shown by complex **17** (injected activity/per gramm IA/g at 23 h after injection was 2.43%) again convince us of the promising potential of copper-containing preparations as diagnostic agents for imaging brain pathologies. Ex vivo biodistribution analysis of **17**-preinjected BALB/C mice bearing EMT6 tumors showed a $4.17\% \pm 1.03\%$ injected activity per gram of tissue at 40 min post-injection, and $4.41\% \pm 0.23\%$ injected activity per gram of tissue in the brain.

Therefore, Cu-ATSM-based agents are interesting both as redox-active agents sensitive to hypoxia, capable of accumulation in solid tumors, and as highly penetrating agents for therapy and diagnostics of brain pathologies.

Conjugates containing A β -binding and metal-chelating moieties were found to modulate the aggregation of A β_{42} species [49,50]. Therefore, ^{64}Cu coordination compounds based on them are expected to bind A β effectively.

Watanabe et al. designed and synthesized two novel ^{64}Cu -labeled benzofuran derivatives **26** and **27** with cyclen (1,4,7,10-tetraazacyclododecane) or DOTA (1,4,7,10-tetraazacyclododecane-1,4,7,10-tetraacetic acid) as chelators [45] (Figure 8).

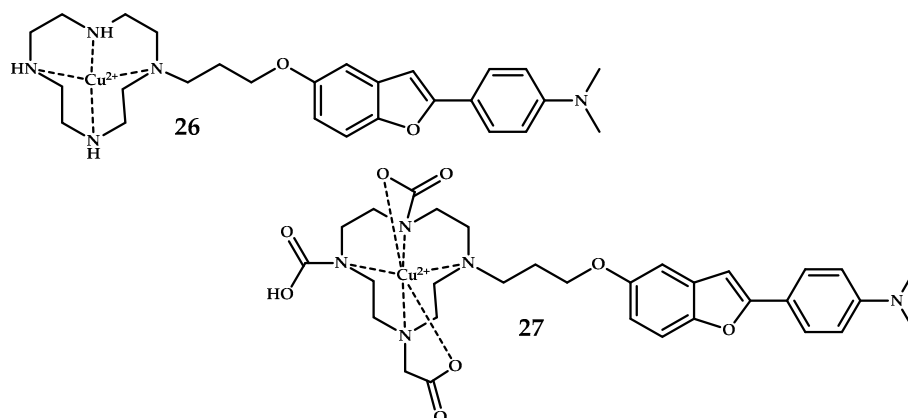


Figure 8. Benzofuran moiety, conjugated with metal-chelating cyclen **26** or 1,4,7,10-tetraazacyclododecane-1,4,7,10-tetraacetic acid (DOTA) **27**, designed for A β fibrils visualization.

An *in vitro* binding assay with $[\text{125I}]6\text{-iodo-2-(40-dimethylamino)-phenyl-imidazo [1,2-a] pyridine}$ [^{125}I] IMPY as the competitive ligand showed dose-dependent inhibition with K_i 33.7 ± 14.6 , 243.5 ± 88.2 . Fluorescent staining using Tg2576 mice brain sections proved the amyloid-binding ability of **26** to a greater extent than **27**. Unfortunately, biodistribution studies revealed quite low brain uptake equal to 0.33% and 0.36%, respectively.

Sharma et al. designed a series of copper-coordination compounds based on an A β -binding 2-phenylbenzothiazole moiety, conjugated with metal-chelating macrocyclic 1,4,7-triazacyclononane (tacn) and 2,11-diaza [3.3]-(2,6)pyridinophane (N_4H_2) **29–33** [46,47] (Figure 9). The ThT fluorescence competition assay suggests a good affinity **L29–L33** for A β_{40} fibrils. Fluorescence microscopy studies on Tg2576 APP Tg-mice brain sections, with amyloid-binding Congo Red as a control, showed a specific binding for organic ligands **L29–L33**. The ThT competition assays with copper complexes **29–33** also revealed a strong A β binding affinity for **32**. A specific binding of the ^{64}Cu -labeled **L29–L33** to A β plaques was proven using *ex vivo* autoradiography studies on brain sections of Tg2576 mice and wild-type mice as a control in the absence and presence of a known A β -specific blocking agent (B1). Coordination compounds **29–33** showed a significant A β binding: the autoradiography intensity markedly decreased in the presence of B1 blocking agent. Biodistribution studies in normal CD-1 mice showed the highest brain uptake of $1.33\% \pm 0.27\%$ ID/g at 2 min post-injection for **29**. The PET/CT imaging of the Tg2576 mice showed a radiotracer accumulation in the head and neck area for **29**, **31**, and **32**. Coordination compound **29** shows the highest brain uptake of $0.57\% \pm 0.05\%$ ID/g in post-PET biodistribution analysis.

Huang et al. developed a series of compounds based on classical amyloid-binding moiety Pittsburgh compound B and used fragments 1,4-dimethyl-1,4,7-triazacyclononane (tacn) as the metal-chelating group [48] (Figure 10). The ThT fluorescence competition assays showed nanomolar affinities for the A β_{1-40} for organic ligands **L34** and **L35**. Staining with 5xFAD mice brain sections showed significant A β -binding affinity of the organic ligands **L34–36** and **L39**. The Cu^{2+} complexes **35**, **36**, and **39** also showed significant A β binding. The MTT (3-(4,5-dimethylthiazol-2-yl)-2,5-diphenyl-2H-tetrazolium bromide) cell viability assays on mice neuroblastoma (N2a) cells showed that coordination compounds **35**, **37**, and **38** exhibit no appreciable cell toxicity. Unfortunately, determination of the octanol/phosphate-buffered saline (PBS) partition coefficient values revealed that ^{64}Cu -labeled complexes **37** and **38** exhibit $\log D_{\text{oct}}$ values of 0.6, suggesting that 2-pyridyl-benzothiazole derivatives may be too hydrophilic to cross the BBB.

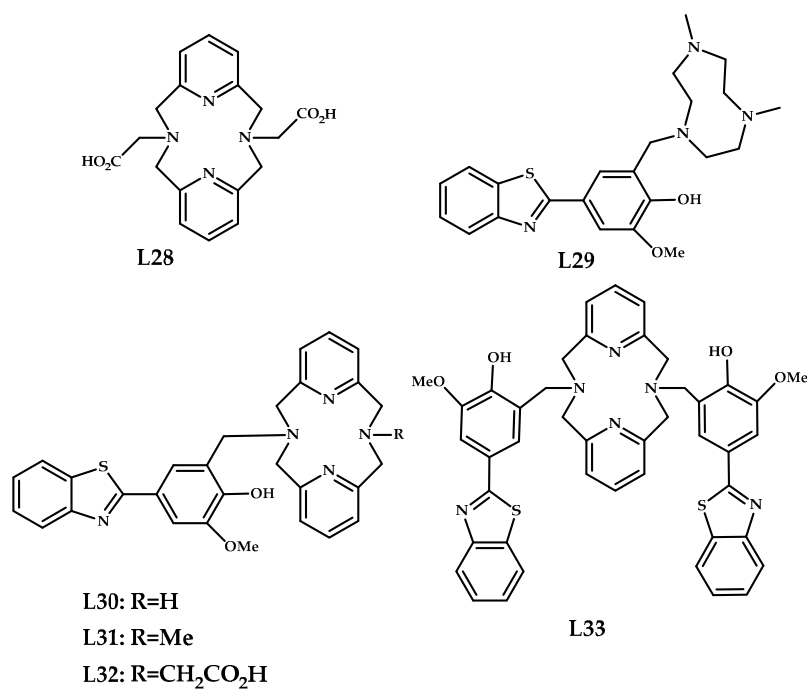


Figure 9. Benzothiazole moieties, conjugated with metal-chelating 1,4,7-triazacyclononane and 2,11-diaza[3.3]-(2,6)pyridinophane **L29–L33**, designed for A β fibrils binding, and model ligand **L28** without benzothiazole moiety.

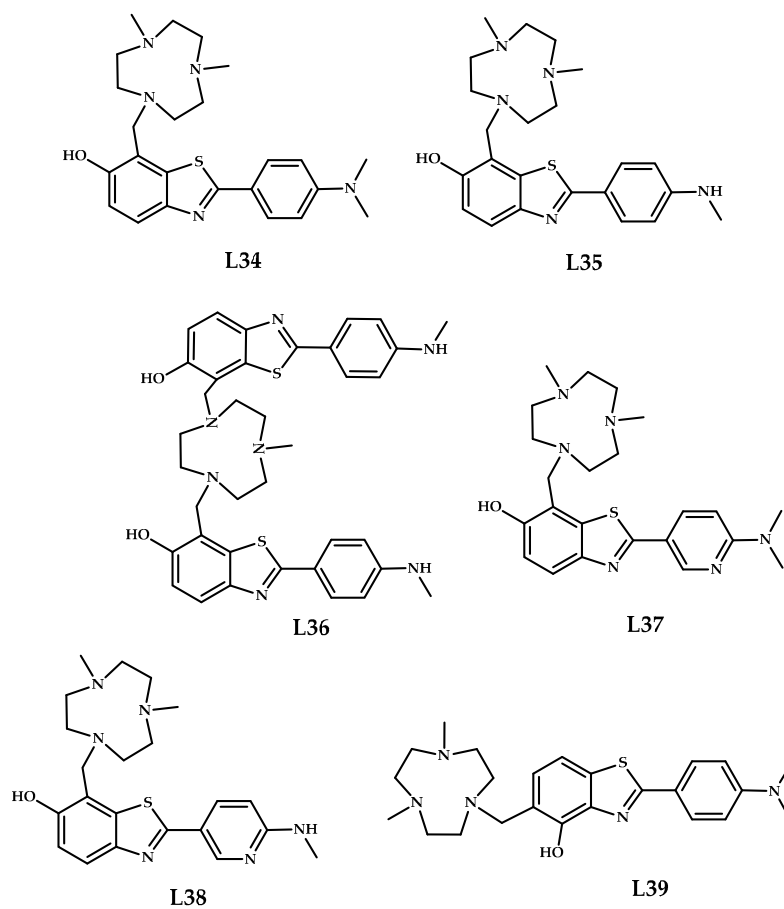


Figure 10. Pittsburg compound B derivatives, conjugated with metal-chelating 1,4-dimethyl-1,4,7-triazacyclononane **L34–L39**, designed for A β fibrils binding.

Ex vivo autoradiography studies using brain sections of 5xFAD Tg-mice confirmed an amyloid-binding specificity of radiolabeled coordination compounds **35**, **36**, and **39**, but ^{64}Cu -labeled **34** also exhibits nonspecific binding. The MW of **36** was found to be too large for efficient brain uptake. Biodistribution studies in normal CD-1 mice proved **39** to cross the BBB, while **35** showed low brain uptake.

3. Gd^{3+} and Ga^{3+} Coordination Compounds for $\text{A}\beta$ Visualization

Another promising emerging radionuclide for PET is ^{68}Ga . Positron-emitting ^{68}Ga can be obtained from a $^{68}\text{Ge}/^{68}\text{Ga}$ generator, which would facilitate cyclotron-independent distribution of PET. The parent nuclide ^{68}Ge has a half-life of 271 days, and the generators can provide sufficient quantities of ^{68}Ga for up to one year, resulting in a relatively inexpensive and reliable source of a positron-emitting radionuclide [51]. Ga^{3+} is a hard acid metal that can make strong bonds with hard base ligands such as carboxylic acids, amino nitrogen hydroxamates, and phenolates [52], which leads to the tendency to use rigid oxygen-containing chelating structures in ^{68}Ga -based drug candidates, such as 1,4,7,10-tetraazacyclododecane-1,4,7,10-tetraacetic acid DOTA.

MRI is an imaging technique based on the physical phenomenon of nuclear magnetic resonance. Various structural and functional changes including atrophy, vascular dysfunction, or changes in the volume of the hippocampus can be quantified using anatomical MRI [53]. Gadolinium(III) is the constituent of most MRI contrast agents due to a large magnetic moment (spin only effective magnetic moment $\mu_{\text{eff}} \frac{1}{4} 7.94 \text{ BM}$, from seven half-filled f-orbitals) and a long electron-spin relaxation time (108 to 109 s, from the symmetric S electronic state) [54]. Table 2 summarizes the coordination compounds for magnetic resonance imaging (MRI) and single-photon emission computed tomography (SPECT) diagnostics of Alzheimer's disease, based on amyloid-affinity ligands conjugated with various metal chelating moieties:

Table 2. Gd^{3+} , Ga^{3+} coordination compounds for magnetic resonance imaging (MRI) and single-photon emission computed tomography (SPECT) imaging of AD.

| No | Brain Uptake, % | Diagnostic Method | Metal | Metal- Chelating Moiety | $\text{A}\beta$ -binding Moiety | Reference |
|----------|--|-------------------|---|--|--|-----------|
| 40–42 | Cellebrium 0.50 ± 0.07 Cortex 0.36 ± 0.03 | MRI SPECT | Gd^{3+} , $^{111}\text{In}^{3+}$ | DO3A | PiB | [55] |
| 43, 44 | - | MRI | Gd^{3+} | DO3A | PiB | [56] |
| 45–60 | - | MRI | Gd^{3+} | DOTA PCTA | Benzothiazole Benzoxazole Stilbene | [57] |
| 61 | - | PET | Ga^{3+} | DOTA | Benzofuran | [58] |
| 62–64 | - | PET | Ga^{3+} | DOTA | PiB | [59] |
| 65–70 | 0.12 ± 0.05 0.17 ± 0.05 0.31 ± 0.09 0.21 ± 0.05 0.22 ± 0.03 0.11 ± 0.01 | PET | Ga^{3+} | HBED-CC | Styrylpyridine | [60] |
| 71 | 1.24 ± 0.31 | PET | Ga^{3+} | | Chalkone | [61] |
| 72 74 | No brain uptake | - | Ga^{3+} | | Curcumin | [62,63] |
| 75 | No biodistribution experiment | - | Ga_3^+ | N_2O_2 Schiff- base ligand | Curcumin | [64] |
| 76, 77 | | - | Ga^{3+} | NODAGA AAZTA | Curcumin | [65] |
| 78–88 | 0.21 ± 0.07 (5 min p.i.) | PET SPECT | Ga^{3+} $^{99\text{m}}\text{Tc}^{3+}$ | DOTA | Tacrine | [66] |

Martins et al. have designed an amyloid-targeted ligand that can efficiently complex different metal ions for various imaging modalities, including Gd^{3+} for MRI and $^{111}\text{In}^{3+}$ for SPECT imaging by a conjugation of a cyclen-based macrocycle DO3A (1,4,7,10-tetraazacyclododecane-1,4,7-triacetic acid) with a benzothiazole moiety [55]. Ligand **L40**-based complexes of Gd^{3+} , Eu^{3+} , and $^{111}\text{In}^{3+}$ were obtained (Figure 11).

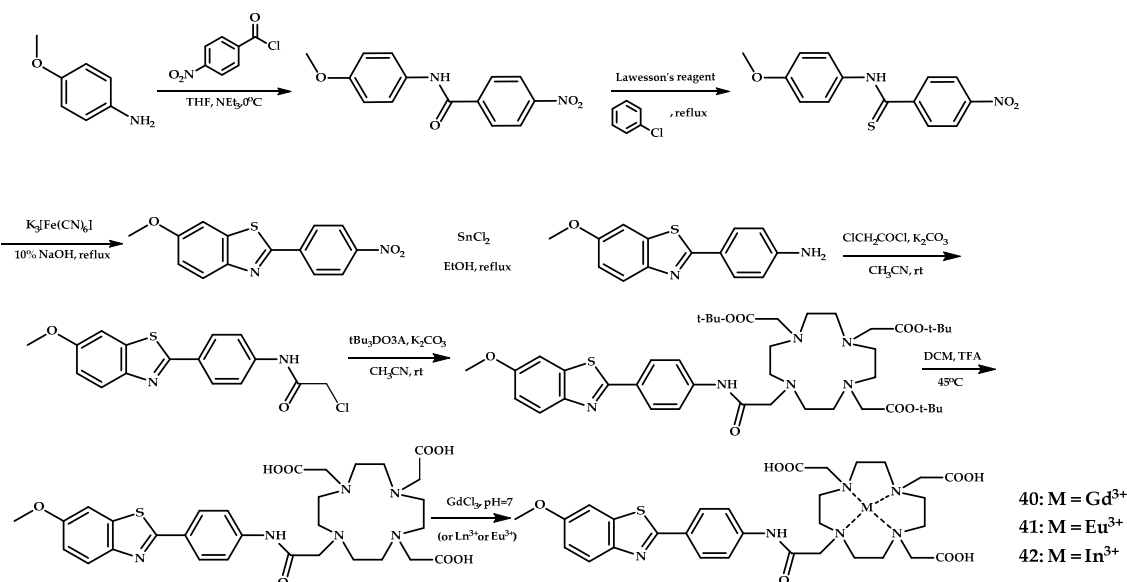


Figure 11. Synthesis of $\text{A}\beta$ -specific DO3A-benzothiazole ligand **L40** and coordination compounds **40** (Gd^{3+}), **41** (Eu^{3+}), and **42** (In^{3+}) based on it, designed for MRI and SPECT $\text{A}\beta$ fibrils visualization.

Upon binding of **40** to $\text{A}\beta$ plaques, higher relaxivity in nuclear magnetic relaxation dispersion (NMRD) profiles was observed due to the complex becoming immobilized during plaque binding. A binding affinity of **40** to $\text{A}\beta_{1-40}$ was evaluated by surface plasmon resonance measurements and yielded $K_d = (180 \pm 10) \mu\text{M}$, and similar K_d values were also expected for the Eu^{3+} and In^{3+} analogues **41** and **42**. The binding affinity of **40** to HSA was assessed by proton relaxation enhancement measurements and yielded $K_d = 110 \pm 20 \mu\text{M}$. A specific binding of **41** to $\text{A}\beta$ deposits was proved on postmortem human brain tissue of AD patients using fluorescence staining with PiB and thioflavin-S as controls. Unfortunately, the $\log P$ oct/water -0.15 value for **40** and also the high MW = 842 shows that the complex is not optimized to cross the BBB. In vivo biodistribution experiments with the radiolabeled ^{111}In -analogue **42** in adult male Swiss mice showed that cortex and cerebellum penetration ID/g at 2 min was 0.36% and 0.5%, respectively.

Martins et al. subsequently presented two novel DO3A monoamide derivative ligands conjugated to the PiB moiety, **43** and **44**, via linkers differing in length and chemical structure to improve the $\log P$ -value and to enhance BBB penetration of the complexes [56] (Figure 12).

The amphiphilic compounds **43** and **44** were found to form micelles in solution. Analysis of the rotational dynamics for micelles formed using the Lipari-Szabo approach indicated highly flexible large aggregates. The coordination compounds **43** and **44** were unable to cross the BBB, and the amount detected was found to be insufficient for MRI detection.

Bort et al. reported amyloid-targeted hydroxybenzothiazole, hydroxybenzoxazole, and hydroxy-trans-stilbene moieties conjugated via neutral and positive-charged linkers with PCTA (3,6,9,15-tetraaza bicyclo[9.3.1]-pentadeca[1(5),11,13-triene-3,6,9-triacetic acid) and DOTA (1,4,7,10-tetraazacyclododecane-1,4,7,10-tetraacetic acid) as metal-chelates, and $\text{Gd}(\text{III})$ complexes **45–60** based on them [57] (Figure 13).

The affinity of the coordination compounds **45–60** for amyloid aggregates was determined in vitro using $[^{125}\text{I}]\text{IMPY}$ ($[^{125}\text{I}]\text{6-iodo-2-(40-dimethylamino)-phenyl-imidazo [1,2-a]pyridine}$)-binding

competition experiments on synthetic A β_{1-42} aggregates, with DOTA-(Lys) $_3$ -BTA being the most potent. To assess the BBB permeability of the coordination compounds, an in vitro model of BBB constituted of a co-culture of rat primary brain capillary endothelial cells and rat glial cells was used. Unfortunately, none of the designed complexes showed BBB penetration ability.

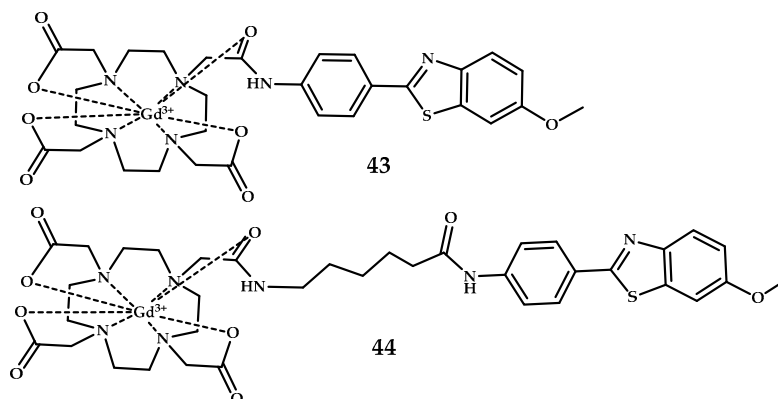


Figure 12. DO3A-PiB-based Gd $^{3+}$ coordination compounds **43** and **44**, designed for MRI visualization of A β plaques.

Watanabe et al. designed and synthesized ^{68}Ga -labeled benzofuran derivative **61** with 1,4,7,10-tetraazacyclododecane-1,4,7,10-tetraacetic acid (DOTA) as the metal-chelating agent [58] (Figure 14). A competitive A β_{1-42} binding experiment of **61** (with [^{125}I] (IMPY) as the competitive ligand) showed a dose-dependent inhibition and values close to the clinically applied IMPY. Neuropathological fluorescent staining of Tg2576 mice brain sections treated with coordination compound **61** with Thioflavin S as a control proved a specific binding of the coordination compound to A β plaques. A biodistribution experiment in normal mice showed brain uptake of the coordination compound **61** (0.45% ID/g), which is too low for the compound to serve as an MRI agent.

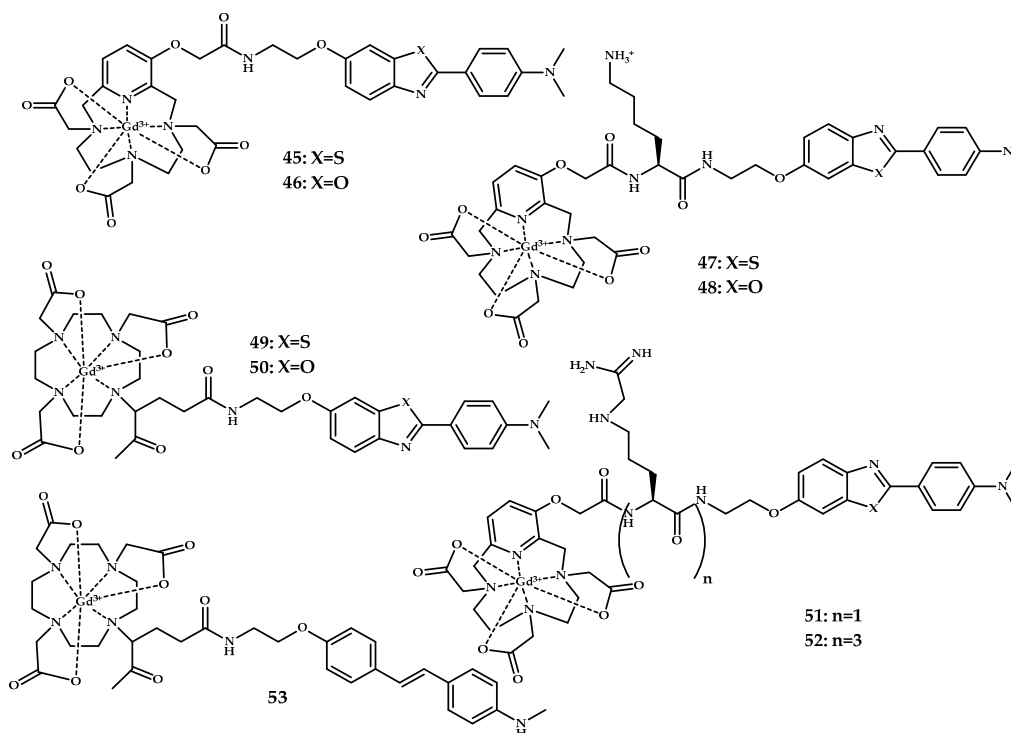


Figure 13. Cont.

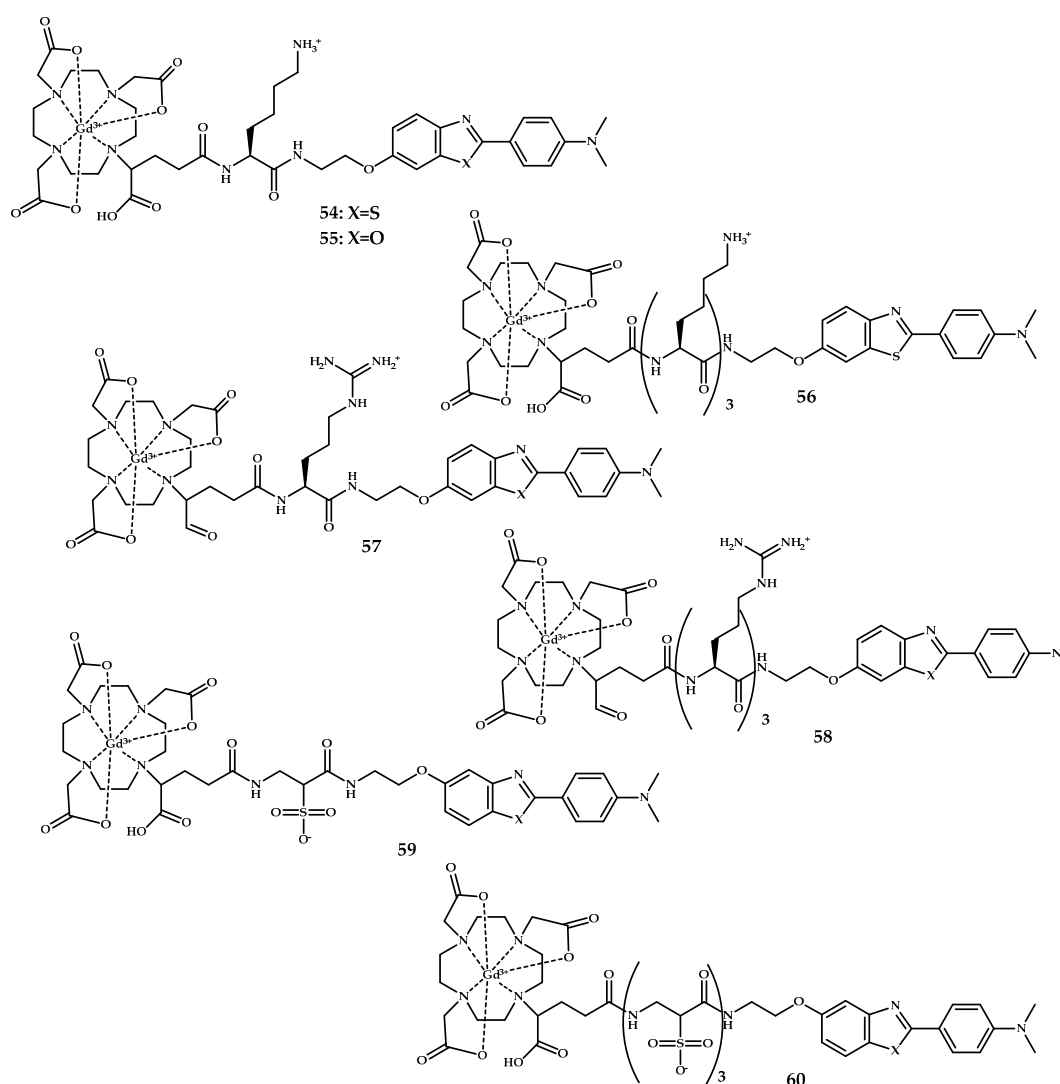


Figure 13. PCTA/DOTA-benzothiazole/benzoxazole/stilbene-based Gd^{3+} coordination compounds 45–60 designed for MRI visualization of $A\beta$ plaques.

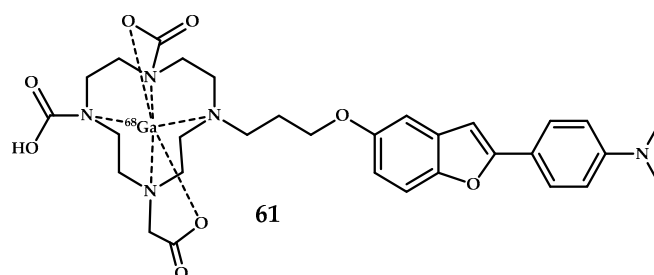


Figure 14. DOTA-benzofuran-based Gd^{3+} coordination compound 61 designed for MRI visualization of $A\beta$ plaques.

Cressier et al. reported ^{68}Ga -labeled complexes conjugated to Pittsburgh Compound B, 2-(4'-[^{11}C]methylaminophenyl)-6-hydroxybenzothiazole (PIB) and DOTA via aromatic or alkyl pacers **L62–L64** [59] (Figure 15). The BBB permeability of the complexes was insufficient, as shown by μ PET. Moreover, the evaluation of the complexes **62–64** through an autoradiographic approach with human brain tissues failed to detect amyloid deposits.

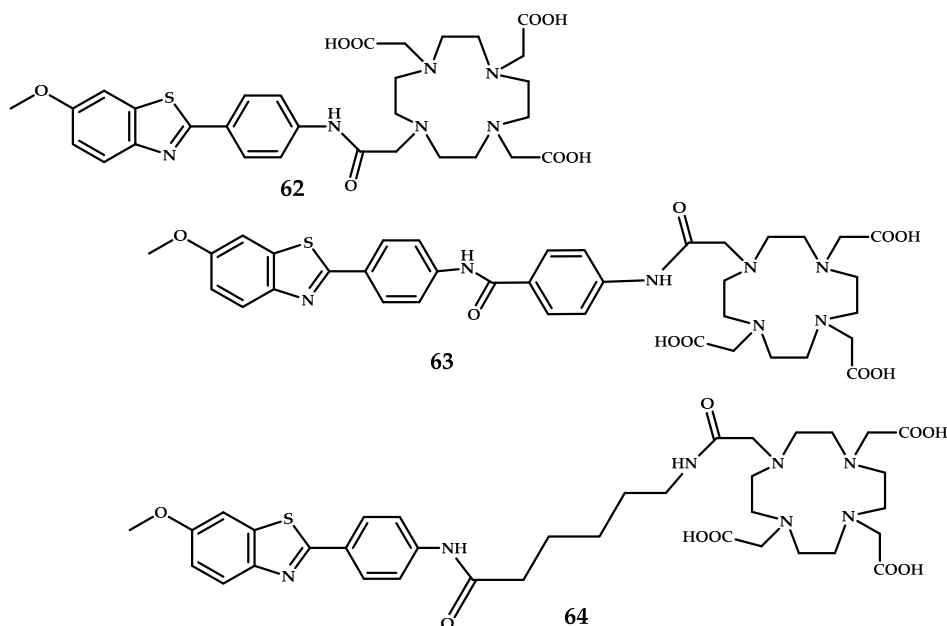


Figure 15. DOTA-Pib-based ligands L62–L64.

Zha et al. reported ^{68}Ga -labeled styrylpyridine derivatives **65–70** with high MW based on an N,N' -bis[2-hydroxy-5-(carboxyethyl)benzyl]ethylenediamine- N,N' -diacetic acid (HBED-CC) core for Ga^{3+} complexation derivatized with styrylpyridinyl groups [60] (Figure 16). An *in vitro* competitive binding assay was conducted to measure the inhibition of [^{125}I]IMPY $\text{A}\beta$ binding by coordination compounds **65–70**. The monovalent conjugate **69** showed a low binding affinity. The *in vitro* autoradiography on AD brain sections showed a high binding affinity of **65–70** to $\text{A}\beta$ plaques, but *in vivo* biodistribution studies in CD-1 mice showed low brain penetration. This may allow a selective labeling of $\text{A}\beta$ plaques deposited on the walls of cerebral blood vessels, which could be a useful tool for diagnosing cerebral amyloid angiopathy (CAA), but not in the $\text{A}\beta$ plaques in the parenchymal brain tissues.

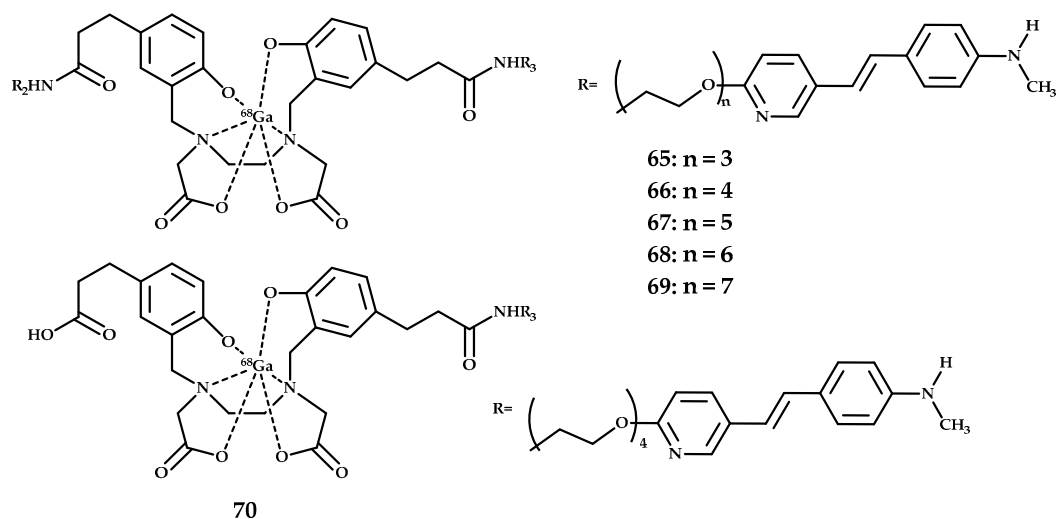


Figure 16. HBED-CC-styrylpyridine coordination compounds **65–70**, designed for PET imaging of $\text{A}\beta$ plaques.

Curcumin (C21), (1E,6E)-1,7-bis(4-hydroxy-3-methoxyphenyl)-1,6-heptadiene-3,5-dione, is a promising organic motif for designing biologically active coordination compounds.

Curcumin demonstrated high antiproliferative activity *in vitro* and *in vivo* [67] and is also known to accumulate in tumor cells, presumably due to the ability to bind the vitamin-D receptor [68].

Curcumin and its derivatives are widely studied as agents for diagnosis, prevention, and treatment of AD [69,70], and also proved to be an amyloid-specific dye [71,72]. It binds to soluble A β plaques [73] and is reported to have sufficient brain permeability and favorable amyloid-binding in *APP^{Sw}* Tg-mice [74]. Curcumin is currently regarded as a specific organic core for AD therapy and diagnostic drug development. Several curcumin-based fluorescent probes for A β imaging have been designed [75]. A number of research works are devoted to a curcumin-based metal-containing agent for MRI, SPECT, and PET diagnostics [76].

The affinity of curcumin for amyloid plaques has raised interest in chalcone derivatives as organic core for the development of A β -affinity diagnostic agents. In 2007, Ono et al. reported chalcone-based probes for *in vivo* imaging of A β plaques in Alzheimer's brains [77]. Chauhan et al. reported a bis-chalcone Ga³⁺-based coordination compound **71** [61] (Figure 17). The stability of coordination compound **69** in HSA was proven using ITLC-SG. Also, the high A β -binding affinity of **69** to HAS was proven in a protein-binding assay. A β -binding studies on aggregated A β ₄₂ were performed, and Scatchard plots suggest one-site binding with a K_d of 3.46 ± 0.41 nM.

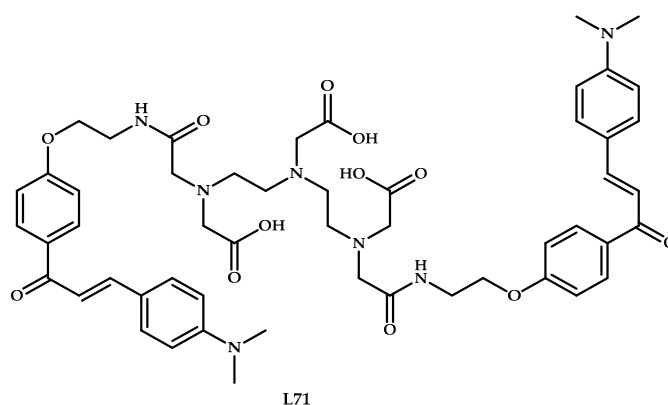


Figure 17. Chalcone-based ligand **L71**, designed for A β plaques binding.

Blood kinetics studies of coordination compound **71** in normal rabbits showed a fast clearance during the initial time period of 30 min. Biodistribution studies showed a high uptake level of 1.24% ± 0.31% with rapid excretion within an hour. Also, PET images in a normal adult male BALB/C mice during 2–30 min intravenous post-injection exhibited a significant activity in the brain at 2 min post-injection and rapid washout from the healthy brain. Thus, coordination compound **71** showed no specific binding or prolonged retention in the healthy brain, due to the absence of A β plaques.

Asti et al. reported ⁶⁸Ga-labeled complexes based on curcumin, diacetyl-curcumin (DAC), and bis(dehydroxy)curcumin (bDHC) **72–74** [62] (Figure 18). The affinity of nat/⁶⁸Ga-Curcuminoid complexes **72–74** for A β _{1–40} amyloid synthetic fibrils was evaluated by measuring the radioactivity of synthetic A β fibrils preincubated with complexes **72–74** and also using fluorescence microscopy with untreated fibrils as a negative control. A fluorescence microscopy study of drug-preincubated A-549 tumor cells confirmed an internalization of Ga³⁺-curcuminoid complexes in lung cancer cells.

Continuing the study, Rubagotti et al. reported [63] an *in vitro* and *in vivo* investigation of the biological properties of coordination compounds **72–74**. The *in vivo* brain uptake was assessed using a Tg2576 mice model. Although A β plaques were clearly visualized after brain section staining with coordination compounds, no brain uptake *in vivo* was observed. These results indicate a high A β -affinity of gallium complexes **72–74** along with an inability of the coordination compounds to cross the BBB *in vivo*.

Lange et al. reported [64] a six-coordinate Ga³⁺ complex **75** based on an N₂O₂ Schiff-base ligand and β -diketone curcumin, which is known to bind to A β plaques because of the structural similarity to

Congo Red [78] (Figure 19). The ability of **75** to bind to A β plaques was assessed using epi-fluorescence microscopy (λ_{ex} = 359 nm, λ_{em} = 461 nm) on AD and age-matched human brain samples with an 1E8-antibody as control. The obtained results allow suggesting some degree of specificity of **73** for A β plaques.

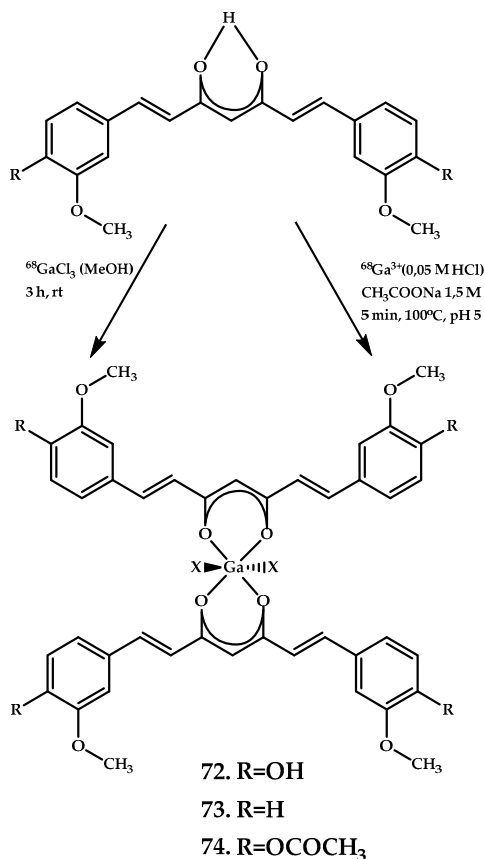


Figure 18. Curcumin-based Ga³⁺ coordination compounds **72–74**, designed for PET imaging of A β plaques.

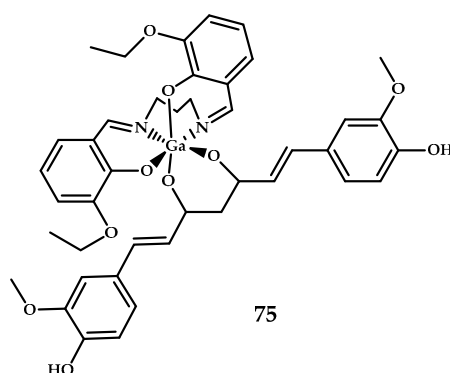


Figure 19. Curcumin-based Ga³⁺ coordination compound **75** with a Schiff-based metal-chelating moiety, designed for PET imaging of A β plaques.

Orteca et al. recently reported curcumin scaffolds conjugated with 1,4,7-triazacyclononane,1-glutaric acid-4,7-acetic acid (NODAGA) and 1,4-bis(carboxymethyl)-6-[bis(carboxymethyl)]amino-6-methylperhydro-1,4-diazepine (AAZTA) as metal chelators **L76** and **L77** [65] (Figure 20).

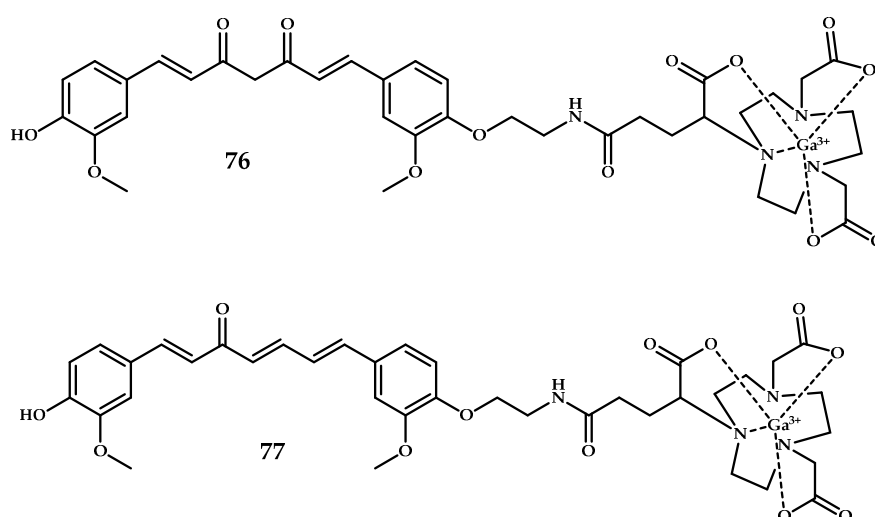


Figure 20. Curcumin-based Ga^{3+} coordination compounds **76** and **77** with NODAGA and AAZTA metal-chelating moieties, designed for PET imaging of $\text{A}\beta$ plaques.

Gniazdowska et al. designed a series of tacrine analogues, acetylcholinesterase (AChE) and butyrylcholinesterase (BuChE) inhibitor [79], the enzymes responsible for the degeneration of the neurotransmitter acetylcholine and labeled with diagnostic radionuclides technetium-99m using bifunctional ligand Hynic [80] **78–85**, and gallium-68, using macrocyclic ligand DOTA **84–86** [80] (Figure 21). The Log D values for the coordination compounds are presented in Table 3. Coordination compounds **82** and **86** with the highest Log D values were selected as lead compounds.

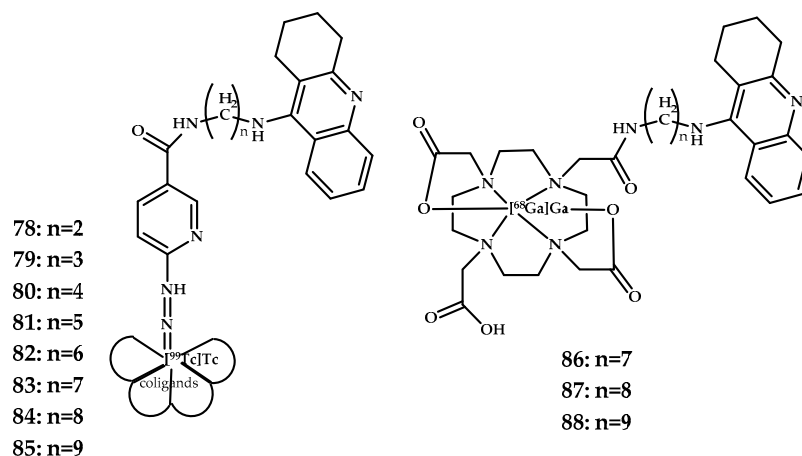


Figure 21. Tacrine-based $^{99\text{m}}\text{Tc}^{3+}$ coordination compounds **78–85** and Ga^{3+} coordination compounds **86–88** with Hynic and DOTA metal-chelating moieties, designed for PET imaging of $\text{A}\beta$ plaques.

Table 3. Log D values for coordination compounds **78–88**.

| $(\text{CH}_2)_n$ | Log D | |
|--------------------|---|--|
| | $[^{99\text{m}}\text{Tc}]\text{Tc-Hynic-NH}(\text{CH}_2)_n\text{Tac}$ | $[^{68}\text{Ga}]\text{Ga-DOTA-NH}(\text{CH}_2)_n\text{Tac}$ |
| 78: $n = 2$ | -2.95 ± 0.06 | - |
| 79: $n = 3$ | -2.80 ± 0.01 | - |
| 80: $n = 4$ | -2.53 ± 0.02 | - |
| 81: $n = 5$ | -2.41 ± 0.01 | - |
| 82: $n = 6$ | -2.08 ± 0.01 | - |
| 83: $n = 7$ | -1.86 ± 0.02 | 86: -2.52 ± 0.01 |
| 84: $n = 8$ | -1.50 ± 0.01 | 87: -2.02 ± 0.01 |
| 85: $n = 9$ | -1.38 ± 0.01 | 88: -1.52 ± 0.01 |

An ability of coordination compounds **82** and **86** to inhibit acetylcholinesterase (AChE) and butyrylcholinesterase (BuChE) was estimated using Ellman's colorimetric assay. The half maximal inhibitory concentration IC_{50} values for the tested derivatives are presented in Table 4. Tacrine was used as the reference inhibitor.

Table 4. The activity of **82** and **86** against two cholinesterases.

| Compound | $IC_{50} \pm SD^{**}$ (nM) | | Selectivity for AChE ^a | Selectivity for BuChE ^b |
|-----------|----------------------------|-------------|-----------------------------------|------------------------------------|
| | AChE | BuChE | | |
| 82 | 0.10 ± 0.01 | 0.12 ± 0.02 | 1.2 | 0.83 |
| 86 | 290 ± 20 | 167 ± 9 | 0.57 | 1.75 |
| Tacrine | 107 ± 9 | 16 ± 1 | 0.15 | 6.67 |

^a Selectivity for AChE is defined as $IC_{50}(\text{BuChE})/IC_{50}(\text{AChE})$; ^b Selectivity for BuChE is defined as $IC_{50}(\text{AChE})/IC_{50}(\text{BuChE})$. ** half maximal inhibitory concentrations ± standard deviation

An in vivo pharmacodynamic study of coordination compound **86** allowed only a qualitative view because the brain penetration was low, 0.21%. The pharmacodynamic study of coordination compound **82** was incomplete due to the low activity of the compound, and the result was therefore omitted. But the ex vivo radioactivity measurement showed that both complexes can penetrate the BBB.

4. $^{99m}\text{Tc}^{3+}$ -Based Coordination Compounds for SPECT Visualization of $\text{A}\beta$

To overcome the limitations of PET imaging in terms of cost and broad accessibility, SPECT was proposed as alternative diagnostic tool [81]. Technetium-99m (^{99m}Tc) is a desirable radioisotope for the preparation of SPECT radiopharmaceuticals because it has a rich chemistry, unique nuclear properties ($T_{1/2} = 6$ h, $E = 140$ keV), and an easy cost-effective availability. ^{99m}Tc can be readily prepared by a $^{99}\text{Mo}/^{99m}\text{Tc}$ generator [82]. The development of a ^{99m}Tc -radiotracer for imaging $\text{A}\beta$ plaques with SPECT is strongly expected to provide a low cost, broadly accessible diagnostic tool for AD. Table 5 summarizes the coordination compounds for single-photon emission computed tomography (SPECT) diagnostics of Alzheimer's disease:

Table 5. ^{99m}Tc coordination compounds for single-photon emission computed tomography (SPECT) visualization of AD.

| No | Brain Uptake, ID/g, 2 Min Post-Injection % | Brain _{2 min} /Brain _{60 min} Ratio | Brain Tissue Experiments | Ligand | Reference |
|--------|--|---|---|--|-----------|
| 89–91 | 4.10 ± 0.38 /6.34 ± 0.81 | 8.20 4.18 1.73 | Fluorescent staining of Re complexes on <i>APP^{swe}/PSEN1</i> mice and AD patient brain sections | Chalcone-mimic moiety with [$^{99m}\text{Tc}(\text{CO})_3$] | [83] |
| | 2.30 ± 0.27 /3.68 ± 0.07 | | | | |
| | 1.11 ± 0.34/ 1.64 ± 0.17 | | | | |
| | With/without PgP Blocked by Cyclosporin A | | | | |
| 92–95 | 0.49 ± 0.08 0.47 ± 0.11 0.48 ± 0.06 0.31 ± 0.06 | 6.13 3.92 5.33 2.06 | In vitro fluorescent staining of Re complexes of brain tissue <i>APP^{swe}/PSEN1</i> mice | Curcumin-like dibenzylideneacetone conjugated with monoamine monoamide dithiol (MAMA) and BAT (bis(aminoethanethiol) as chelating moieties | [84] |
| | | | | | |
| | | | | | |
| | | | | | |
| 96–100 | 0.28 ± 0.03 | 2.54 | Autoradiography <i>Tg2576</i> and wild-type mice | Benzotiasole/stilbene conjugated with hydroxamamide (Ham) as chelating moiety | [85,86] |

Table 5. Cont.

| No | Brain Uptake, ID/g, 2 Min Post-Injection % | Brain _{2 min} /Brain _{60 min} Ratio | Brain Tissue Experiments | Ligand | Reference |
|----------|--|--|--|---|-----------|
| 101–104 | 0.25 ± 0.05 0.24 ± 0.02 (wild type/ <i>APP</i> mice) | 1.26 | SPECT images in <i>APP/PS1</i> transgenic mice | Styrylpyridyl conjugated with pyridylamine-carboxylate and dipyrildylamine ligands as chelating moiety | [87] |
| 105–107 | 1.10 ± 0.08 0.96 ± 0.13 1.55 ± 0.51 1.24 ± 0.17 | 3.54 6.40 3.87 8.64 | In vitro autoradiography Brain tissue from <i>APP^{swe}/PSEN1</i> mice | Arylbenzoxazole conjugated with bis (aminoethanethiol) (BAT) as chelating moiety | [88] |
| 109–116 | 0.80 ± 0.17 0.61 ± 0.08 0.88 ± 0.14 1.21 ± 0.22 | 26.66 3.38 6.68 20.16 | Fluorescent staining of Re complexes with brain sections of <i>APP^{swe}/PSEN1</i> mice and AD patients In vitro autoradiography on brain sections of <i>APP^{swe}/PSEN1</i> mice and AD patients | Benzothiazole conjugated with iminodiacetic acid (IDA) as chelating moiety | [89] |
| 117–132 | 0.69 ± 0.16 0.46 ± 0.09 0.59 ± 0.12 2.11 ± 0.11 0.92 ± 0.09 0.47 ± 0.07 0.60 ± 0.05 | 1.50 1.15 1.37 3.40 1.46 2.47 2.07 | Fluorescent staining of rhenium complexes on brain slices from <i>APP^{swe}/PSEN1</i> mice and AD patients. Autoradiography on brain slices from <i>APP^{swe}/PSEN1</i> mice Ex vivo Autoradiography <i>APP^{swe}/PSEN1</i> mice In vivo SPECT–CT Imaging in Rhesus Monkeys | Arylbenzoxazole conjugated with bis (aminoethanethiol) (BAT) as chelating moiety | [90] |
| 131 | - | - | Fluorescent staining or De complexes of AD human brain tissue | Styrylpyridyl conjugated with 2-aminoethyl-2-hydroxybenzamide as chelating moiety | [91] |
| 132 | 0.53 ± 0.11 0.52 ± 0.08 (healthy/5x <i>FAD</i> mice) | Brain _{2 min} /Brain _{90 min} 2.0 Brain _{2 min} /Brain _{90 min} 2.1. | Fluorescence staining of Re complexes of AD patient brain and 5x <i>FAD</i> mice | Benzothiazole conjugated with tricarbonyl [M(CO) ₃] ⁺ | [92] |
| 133–135 | 0.88 ± 0.08 | 3.52 | Ex vivo autoradiography using Tg2576 mice | Phenylquinoxaline conjugated with bis (aminoethanethiol) (BAT) as chelating moiety | [93] |
| 136–140 | - | - | Fluorescence staining of Re complexes of AD patient brain | Styrylpyridyl/Benzofuran conjugated with pyridylthiosemicarbazide as chelating moiety | [94] |
| 141, 142 | 0.78 ± 0.07 0.86 ± 0.07 | 8.66 7.16 | Autoradiography of AD rat model (vaccinated with Aβ solution) | Arylimidazo[2,1-b] benzothiazole conjugated with triazole-based N/N/O, N/N/N, N/N/S ligands as chelating moieties | [95] |
| 143–145 | 7.94 ± 1.46 3.99 ± 0.60 5.36 ± 0.65 | 39.7 99.75 59.55 | Fluorescent staining of AD patient brain | Benzothiazole with benzene ring replaced by the cyclopentadienyl tricarbonyl | [96] |
| 146 | 0.38 ± 0.03 0.35 ± 0.01 (AD/normal rats) With/without blocked PgP (Cyclosporine A) (10 min after injection) 0.27 ± 0.01 0.60 ± 0.01 | Brain _{2 min} /brain _{30 min} 2.33 Brain _{2 min} /brain _{30 min} 1.65 | Planar scintigraphy, autoradiography and fluorescent staining with Thioflavin S and Congo Red studies on prepared brain slices of AD rats (vaccinated with Aβ1–42) and brain sections of AD and Schizophrenia patients. | D-(FPLIAIMA)-NH ₂ peptide | [97] |

Liu et al. designed and synthesized novel chalcone-mimic Re/^{99m}Tc **Re-89–91**/^{99m}Tc**[87–91]** complexes [83] (Figure 22). Ferrocene complexes were synthesized as precursors for ^{99m}Tc coordination

compounds. Complexes **Re-90** and **Re-91** demonstrated a high affinity to A β plaques in brain tissue sections from AD patients and Tg-mice (*APP^{swe}/PSEN1*), while demonstrating no apparent labeling in both normal mice C57BL6 and normal adult brain sections. The K_i value ranges established using an A β_{1-42} binding assay ranged from 899 to 108 nM. As an extension of the conjugated π system, complex **Re-91** demonstrated the highest affinity. The in vitro autoradiography of [^{99m}Tc]**89–91** on Tg-mice brains confirmed the A β affinity of [^{99m}Tc]**91** ($K_i = 108$ nM). In the biodistribution studies, [^{99m}Tc]**89** and [^{99m}Tc]**90** showed excellent initial uptakes and fast clearance (respectively 4.10% and 2.30%) in the brain, while [^{99m}Tc]**91** showed moderate brain uptake (1.11%).

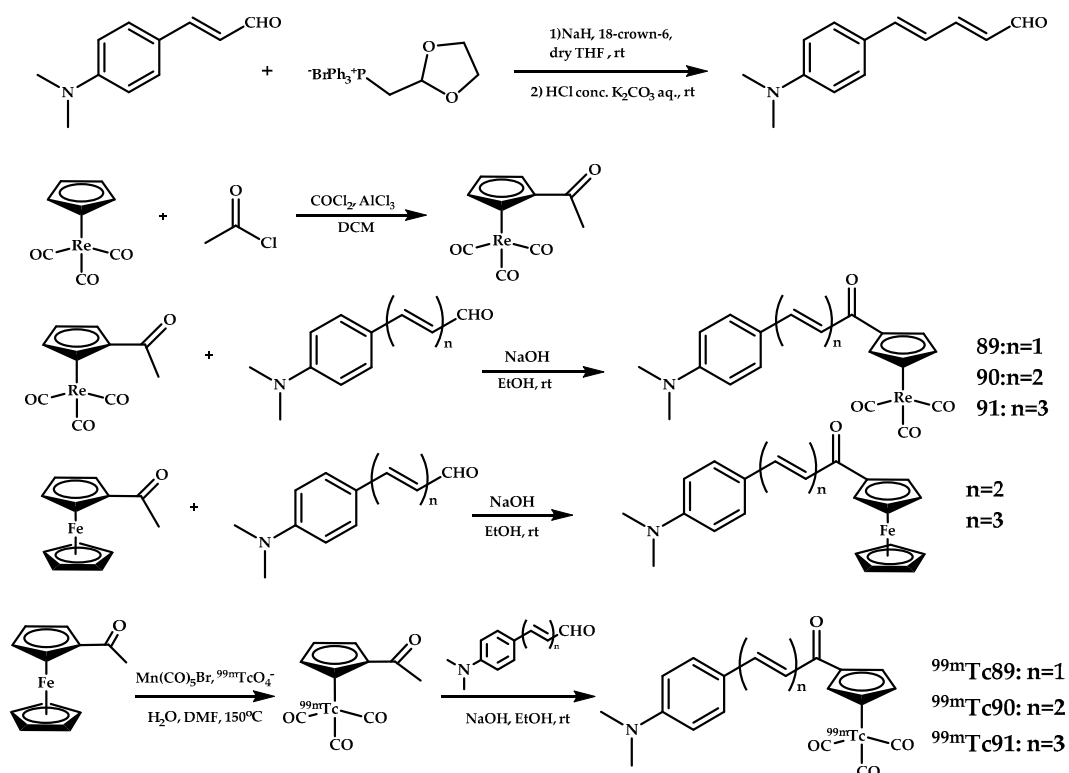


Figure 22. [^{99m}Tc] coordination compounds [^{99m}Tc]**89–91** based on chalcone-mimic scaffolds and their Re analogues **89–91**.

A biodistribution in permeability-glycoprotein blocked by cyclosporin A (an immunosuppressant drug) revealed an increase of BBB-penetrating abilities of the coordination compounds [^{99m}Tc]**89–91**. This result may reveal [^{99m}Tc]**89–91** to be substrates for the rodent PgP transporter.

Yang et al. reported four ^{99m}Tc -labeled dibenzylideneacetone derivatives [^{99m}Tc]**92–95** and corresponding rhenium complexes **92–95** [84] (Figure 23).

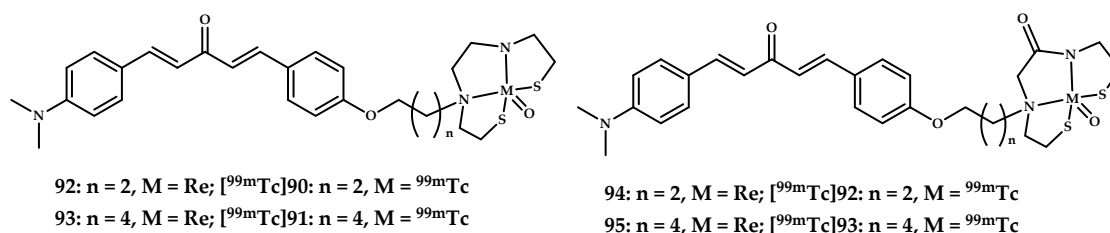


Figure 23. Coordination compounds $\text{Re}/^{99m}\text{Tc}$ **92–95** based on dibenzylideneacetone scaffolds with BAT (**92**, **93**/[^{99m}Tc]**92**, [^{99m}Tc]**93**) and MAMA (**94**, **95**/[^{99m}Tc]**94**, [^{99m}Tc]**95**) designed for SPECT imaging of A β plaques.

The binding affinities of rhenium complexes **92–95** for A β _{1–42} aggregates were evaluated by competition binding assay using [¹²⁵I]IMPY. Coordination compounds **92** and **93** with the BAT chelating moiety showed better A β _{1–42} affinity (K_i = 24.7 and 13.6 nM) compared with coordination compounds **94** and **95** with the MAMA chelating moiety (K_i = 120.9 and 59.1 nM). Increasing the length of the spacer was found to promote A β _{1–42} binding. All four rhenium complexes, **92–95**, displayed excellent labeling of A β plaques in in vitro fluorescent staining on sections of brain tissue from a Tg-mice (C57BL6, *APP^{swe}/PSEN1*) and age-matched control mice. Biodistribution experiments of ^{99m}Tc-labeled coordination compounds [^{99m}Tc]**92–95** in normal ICR mice showed the highest initial uptake at 2 min post-injection (respectively 0.49%, 0.47%, 0.48%, and 0.31% ID/g), followed by rapid washout from the brain.

Iikuni et al. designed five novel ^{99m}Tc-HAM complexes [^{99m}Tc]**96–99** with a bivalent amyloid ligand based on stilbene/benzothiazole moieties and HAM as chelating agent [85] (Figure 24).

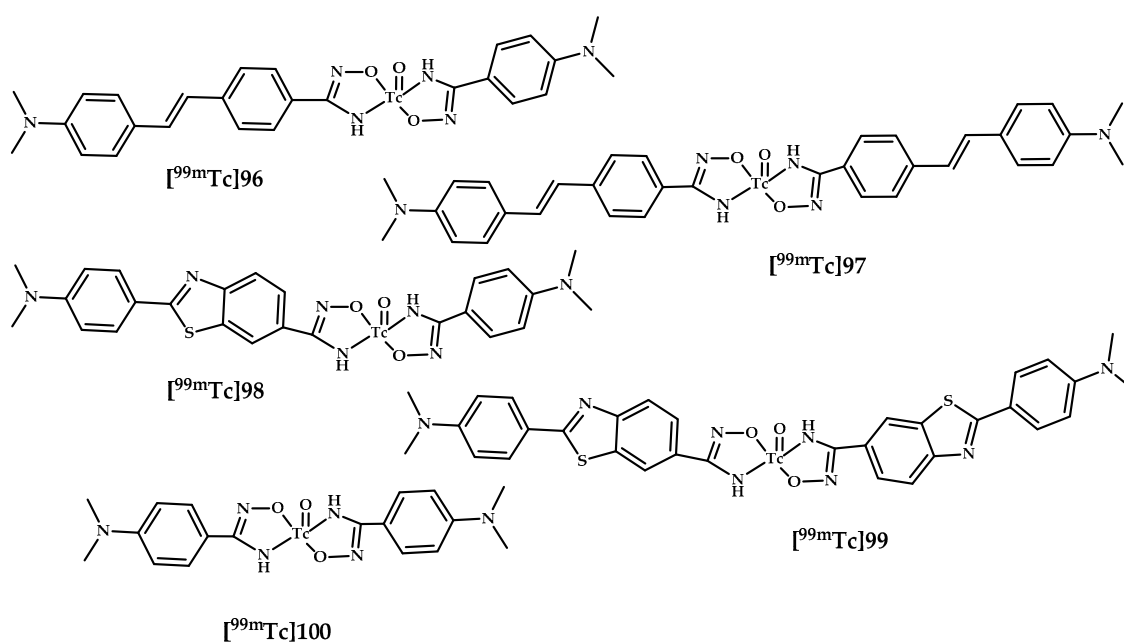


Figure 24. ^{99m}Tc-HAM complexes based on stilbene and benzothiazole moieties [^{99m}Tc]**96–99**, designed for SPECT imaging of A β plaques, and model coordination compound **100**.

Coordination compounds [^{99m}Tc]**96–99** displayed moderate affinity for amyloid aggregates (respectively 22.2%, 42.6%, 4.6%, 38.7%), while model compound [^{99m}Tc]**100**, which does not include any amyloid ligands, showed no affinity. In vitro autoradiography of Tg2576 mice brain section assay proved an ability of [^{99m}Tc]**96**, [^{99m}Tc]**97**, and [^{99m}Tc]**99** to bind A β plaques. A biodistribution experiment of [^{99m}Tc]**97** with the highest binding affinity in the inhibition assay in normal mice showed very low brain uptake (0.28% ID/g).

Further, the authors of Reference [86] applied coordination compounds [^{99m}Tc]**96–99** to CAA-specific imaging probes and evaluated their utility for CAA-specific imaging. An in vitro inhibition assay using A β _{1–40} aggregates deposited mainly in CAA showed a high binding affinity of coordination compounds [^{99m}Tc]**96–99**. In vitro autoradiography of human CAA brain sections and ex vivo autoradiography of Tg2576 mice displayed excellent labeling of A β depositions in human CAA brain sections and high affinity and selectivity to CAA in Tg-mice of coordination compounds [^{99m}Tc]**97** and [^{99m}Tc]**99**.

Hayne et al. reported [87] tridentate ligands **L101–L104** designed to bind to the [M(CO)₃]⁺ core (M = Tc/Re) conjugated with a stilbene A β -binding moiety (Figure 25). The complexes **101** and **103** showed little to no plaque binding in brain tissue from AD-positive subjects. Epi-fluorescence

microscopy of tissue sections of the frontal cortex of an AD-affected brain treated with **102** and **104** bearing an electron-donating dimethylamino functional group revealed good correlation of the complexes to A β plaques, and the E18 antibody was used as a control.

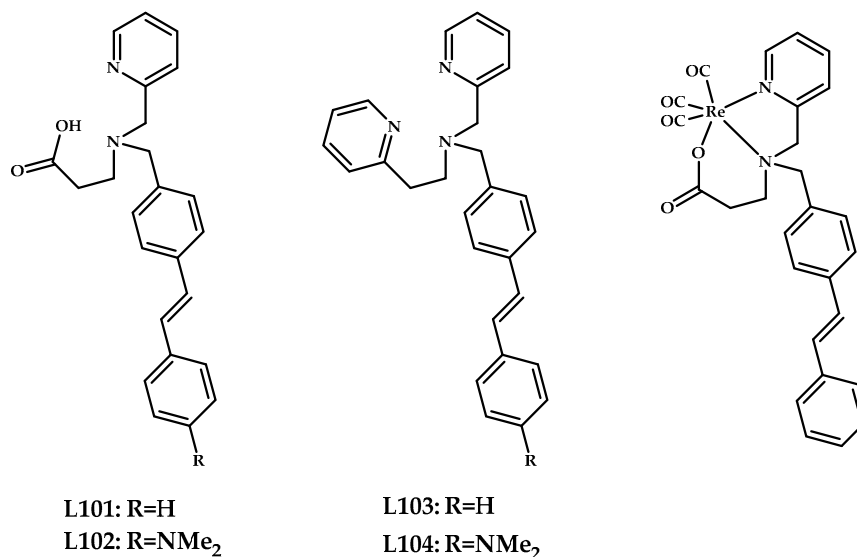


Figure 25. Tridentate ligands **L101–L104** conjugated with a stilbene A β -binding moiety designed for A β plaques binding, and the proposed structure of coordination compound **101**.

The biodistribution of the radiolabeled coordination compound [^{99m}Tc]**103** was investigated in both wild-type and *APP/PS1* Tg-mice. Low brain uptake (~0.25%) was registered in both cases, and no statistically significant difference between wild-type and Tg-mice was observed.

Wang et al. reported four neutral Re/^{99m}Tc-labeled coordination compounds **105–108**/^{99m}Tc] **105–108** based on arylbenzoxazole moieties conjugated with bis(aminoethanethiol) (BAT) as a chelating moiety [88] (Figure 26).

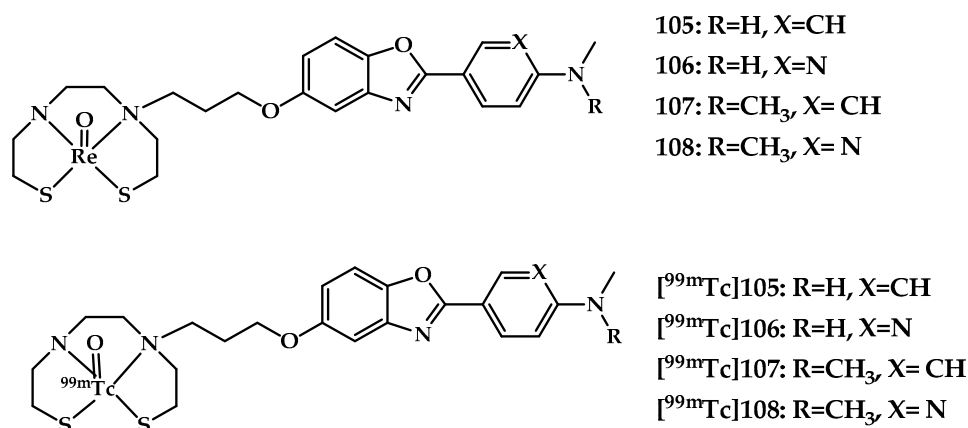


Figure 26. Re³⁺ (**105–108**) ^{99m}Tc³⁺ ([^{99m}Tc]**105–108**) complexes based on arylbenzoxazole with a BAT metal-chelating moiety, designed for SPECT imaging of A β plaques.

In vitro fluorescent staining with rhenium complexes **105–108** with A β plaques, neuropathological staining with the brain sections of a Tg-mice and an AD patient showed specific A β -binding of the complexes. An in vitro competition binding assay was performed using [¹²⁵I] IMPY as the competing radioligand. A moderate A β -binding affinity of **105** and **106** (K_i = 128.21 and 393.18 nM) and a high affinity of complexes **107** and **108** (K_i = 15.86 and 37.19 nM) with N,N-dimethyl amino

group was estimated. ^{99m}Tc -labeled complexes were prepared by a ligand exchange reaction from the intermediate ^{99m}Tc -glucoheptonate. In vitro autoradiography in Tg-mice brain tissue showed labeling of cortex, hippocampus, and cerebellum regions by [^{99m}Tc]107. Biodistribution studies of coordination compounds displayed higher initial brain uptake of N,N-dimethylated derivatives and brain_{2min}/brain_{60min} ratio than the N-monomethylated analogs ([^{99m}Tc]105 vs [^{99m}Tc]107 and [^{99m}Tc]106 vs [^{99m}Tc]108).

Jia et al. reported a design and biological evaluation of a series of negatively charged imaging probes with limited BBB penetration for the selective detection of vascular A β deposition [89]. Eight $^{99m}\text{Tc}(\text{CO})_3$ -labeled benzothiazole derivatives [^{99m}Tc]109–116 and their Re(III) analogues 109–116 were designed as potential SPECT imaging probes for cerebrovascular A β deposition (Figure 27). Rhenium surrogates 109–116 displayed high affinities to A β aggregates with K_i values ranging from 42 to 106 nM, rhenium complex 116 with the longest carbon linker length ($n = 6$) displayed the highest affinity to A β_{1-42} aggregates ($K_i = 42.2$ nM). Complex 115 also demonstrated unambiguous and specific labeling of A β plaques in brain sections from Tg-mice. ^{99m}Tc -labeled coordination compounds [^{99m}Tc]109–116 were obtained by ligand exchange reactions with $\text{fac-}[^{99m}\text{Tc}(\text{CO})_3(\text{H}_2\text{O})_3]^+$.

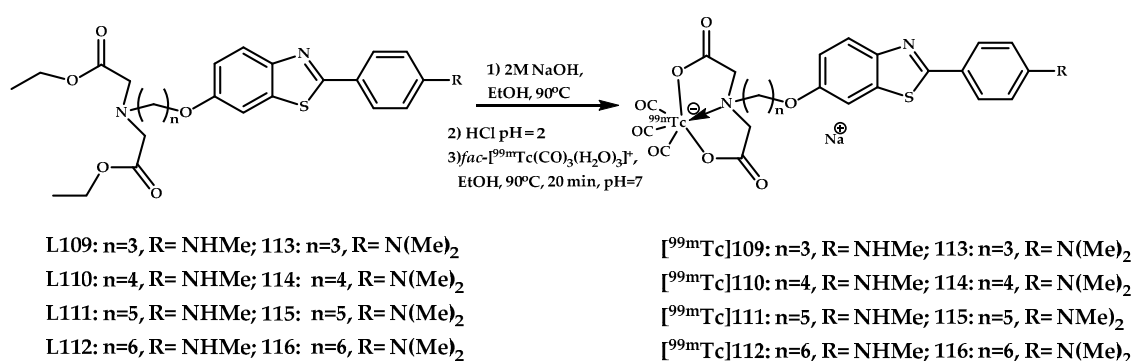
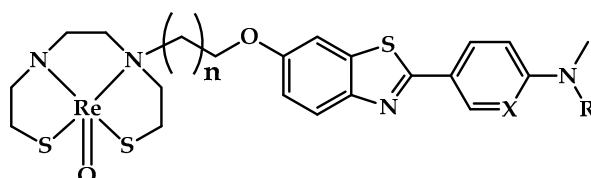


Figure 27. Negatively charged imaging probes [^{99m}Tc]109–116 designed for the selective detection of vascular A β deposition, and their Re^{3+} analogues 109–116.

Autoradiography studies in AD human brain tissue proved the ability of coordination compound [^{99m}Tc]116 to bind A β deposits in blood vessels but not in cerebral parenchyma on brain sections of an AD patient, while [^{125}I]IMP labeled both. Ex vivo autoradiography studies in Tg-mice and wild-type mice were also performed. The radioactive spots were found to concentrate at the site of the blood vessels in the Tg-mice brain tissue, as identified by in vitro fluorescence staining using thioflavin-S. Biodistribution studies of [^{99m}Tc]116 show a relatively low brain uptake equal to $1.21\% \pm 0.22\%$ ID/g at 2 min post-injection and rapid blood washout with an approximately 23-fold decline in blood radioactivity at 60 min post-injection. Other complexes showed worse brain uptake. The authors claimed that coordination compounds [^{99m}Tc]109–116 are prospective as cerebrovascular A β -visualization agents.

Zhang et al. designed a series of sixteen ^{99m}Tc -labeled imaging probes [^{99m}Tc]117–132 for A β plaques based on 2-arylbenzothiazoles conjugated with a bis(aminoethanethiol) (BAT) chelating moiety and their Re(III) analogues 117–132 [90] (Figure 28). An in vitro binding affinity of rhenium complexes 117–132 to aggregated A β_{1-42} peptide was estimated by a competitive binding assay using [^{125}I]IMPY as a reference ligand. The results obtained proved that both the introduction of a dimethylamine group and an increase in the length of the linker between the amyloid affinity and the metal-chelating moiety promotes A β binding of the resulting coordination compounds. Compounds 120 and 122 showed a binding affinity (respectively 8.4 and 8.8 nM) surpassing that of IMPY, a widely used imaging agent. Binding of the coordination compound to A β plaques in Tg-mice and AD brain tissue samples was also proven using in vitro fluorescent staining with thioflavin-S as a control.

^{99m}Tc -labeled probes [^{99m}Tc]**117–132** were obtained using a ligand exchange reaction with ^{99m}Tc -glucoheptonate. The ability of the purified ^{99m}Tc -labeled probes [^{99m}Tc]**118–134** to bind A β plaques was tested in brain slices from Tg-mice. Biodistribution studies of ^{99m}Tc -labeled complexes were conducted. [^{99m}Tc]**124** indicated its suitability as a diagnostic probe. ^{99m}Tc -labeled coordination compound [^{99m}Tc]**124** showed relatively high initial brain uptake (2.11% ID/g at 2 min) and a reasonable clearance rate (0.62% ID/g at 60 min), in contrast to other complexes, which exhibited poor brain uptake (less than 1% ID/g at 2 min) and slow clearance, presumably because of their higher lipophilicity and nonspecific binding to plasma proteins.



117–120: $n = 2–5$, $X = \text{CH}$, $R = \text{CH}_3$

121–124: $n = 2–5$, $X = \text{CH}$, $R = \text{H}$

125–128: $n = 2–5$, $X = \text{N}$, $R = \text{CH}_3$

129–132: $n = 2–5$, $X = \text{N}$, $R = \text{H}$

Figure 28. Re(III) coordination compounds **117–132** based on 2-arylbenzothiazoles conjugated with a BAT chelating moiety.

SPECT images of coordination compound [^{99m}Tc]**122** in rhesus monkeys were registered, and the images revealed radioactivity accumulation in the brain, indicating permeation of [^{99m}Tc]**121** through the BBB (Table 6). This is the first assessment of a ^{99m}Tc -labeled A β probe in nonhuman primates.

Table 6. [^{99m}Tc]**122** brain accumulation in rhesus monkeys (M04: 4-year-old, male; F27: 27-year-old, female).

| | 0–10 Min | 10–20 Min | 20–30 Min | 30–40 Min | Clearance Ratio |
|-----|----------|-----------|-----------|-----------|-----------------|
| M04 | 1.23 | 1.13 | 1.01 | 0.88 | 1.40 |
| F27 | 0.78 | 0.70 | 0.67 | 0.64 | 1.22 |

Hayne et al. reported oxotechnetium(V) and oxorhenium(V) complexes [^{99m}Tc]**133** and **133** based on a styrylpyridyl functional group with 2-aminoethyl-2-hydroxybenzamide as a chelating moiety [91] (Figure 29). The affinity of **133** for A $\beta_{1–42}$ fibrils was estimated to be $K_i = 855$ nM using a fluorescence competition assay against Thioflavin T. It was also shown that **133** binds to A β plaques in human brain tissue using human AD brain sections.

Kiritzis et al. reported a 2-(4'-aminophenyl)benzothiazole-based ^{99m}Tc -radioagent [^{99m}Tc]**134** and its Re(III) analogue **134** [92] (Figure 30). A strong affinity of **134** for A β plaques in brain sections from an AD patient was proven using confocal microscopy. The binding affinity of **134** for A β_{42} was measured in vitro by competition binding assay between the stable **134** and its radioactive ^{99m}Tc -labeled analogue [^{99m}Tc]**134**, and the obtained K_i was 13.6 ± 4.8 nM.

Biodistribution experiments of [^{99m}Tc]**134** in Swiss albino mice revealed a moderate initial brain uptake of 0.53% ID/g at 2 min and slow clearance of radioactivity from the brain with a $\text{brain}_{2\text{min}}/\text{brain}_{90\text{min}}$ ratio of 2.1. Administration of [^{99m}Tc]**134** in 5xFAD Tg-mice showed that 0.52% ID/g of radioactivity is recorded in the brain at 2 min, a result similar to that in healthy mice. But the significant increase of radioactivity in the brain of 5xFAD Tg-mice with time (1.94% ID/g at 90 min post-injection) is consistent with retention of [^{99m}Tc]**134** through binding to A β plaques.

Iikuni et al. reported three novel ^{99m}Tc complexes [^{99m}Tc]**135–137** based on a phenylquinoxaline scaffold and their model Re(III) analogues **135–137** [93] (Figure 31).

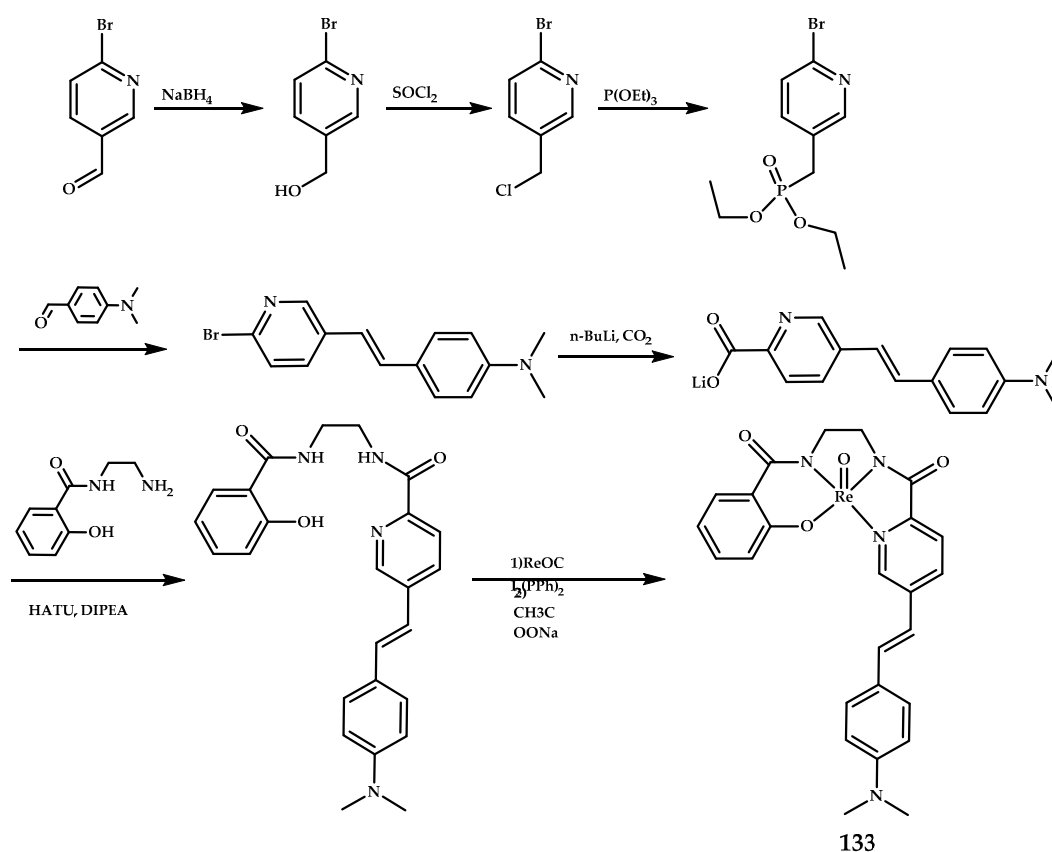


Figure 29. Oxorhenium(V) complexes **133** based on a styrylpyridyl functional group with 2-aminoethyl-2-hydroxybenzamide as a chelating moiety, designed for SPECT imaging of A β plaques.

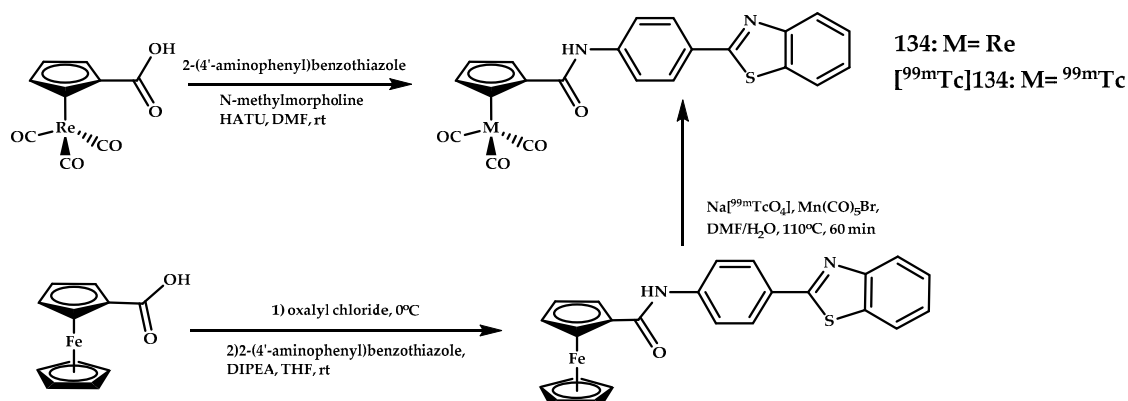


Figure 30. 2-(4'-aminophenyl)benzothiazole-based ^{99m}Tc-radioagent [^{99m}Tc]**134** and its Re(III) analogue **134**, designed for SPECT imaging of A β plaques.

An *in vitro* binding experiment in solution showed promising A β affinity for complex **135** and average binding affinity for complex **136**. The affinity increased in the order of the N,N-dimethylated derivative > N-monomethylated derivative > primary amino derivative.

The brain uptake for ^{99m}Tc-labeled complex [^{99m}Tc]**135** was found to be 0.88%, and the brain_{2min}/brain_{60min} ratio was 3.52. An *ex vivo* autoradiographic examination was also performed using a Tg2576 mice, and [^{99m}Tc]**135** showed intensive radioactive spots in sections from the Tg2576 mice but not from the age-matched mice. In addition, these spots corresponded with A β depositions confirmed by fluorescent staining in the same sections with thioflavin-S.

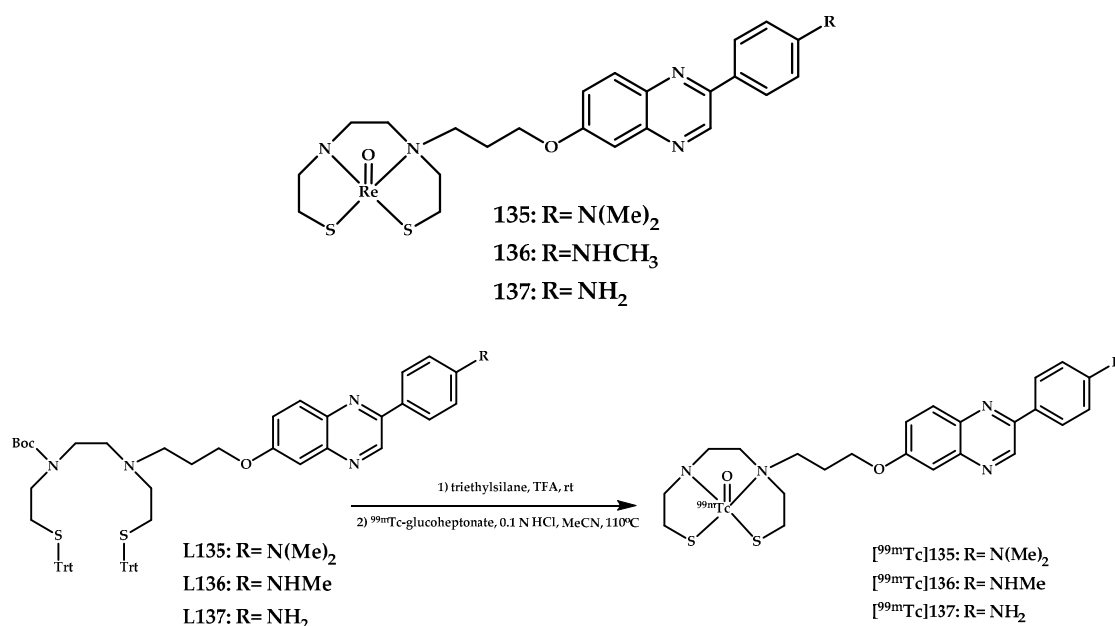


Figure 31. ^{99m}Tc complexes [^{99m}Tc]135–137 based on a phenylquinoxaline scaffold and their model Re(III) analogues 135–137, designed for SPECT imaging of Aβ plaques.

Fletcher et al. reported six Re(III) complexes **138–142** based on styrylpyridyl and benzofuran moieties [94] (Figure 32). An affinity to Aβ plaques was investigated using a ThT assay, and the obtained results suggested that the complexes either bind competitively with ThT to Aβ_{1–42} fibrils or inhibit fibril formation. ^{99m}Tc-labeled coordination compounds [^{99m}Tc]138 and [^{99m}Tc]139 were also obtained.

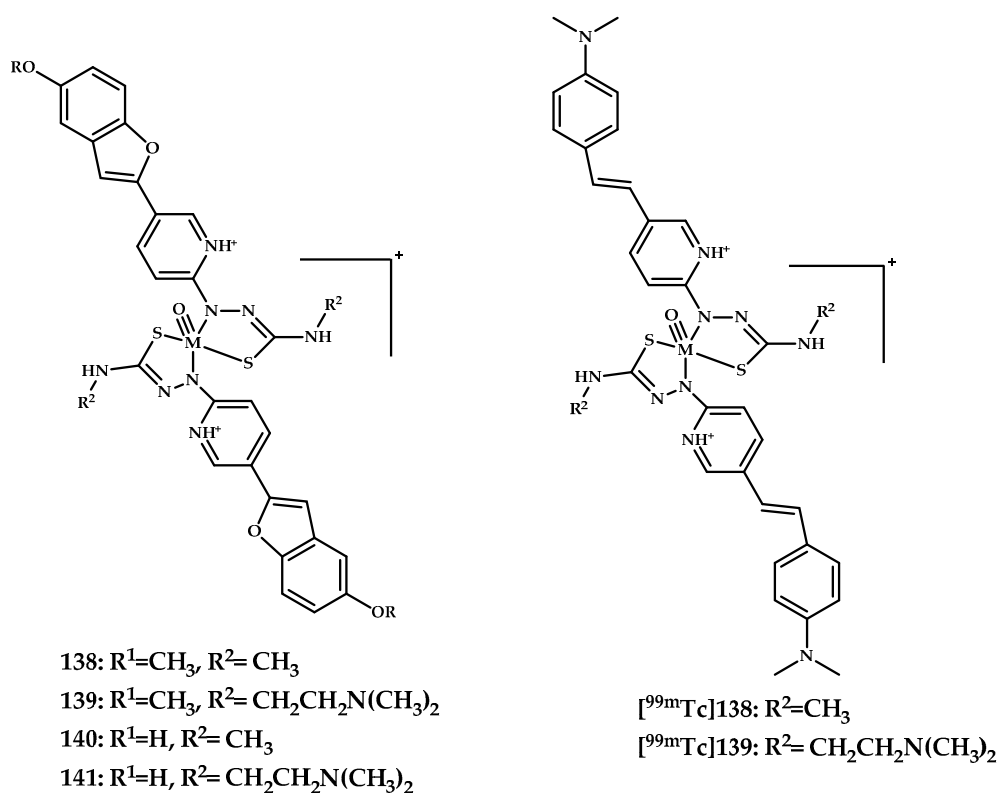


Figure 32. Re(III) complexes **138–142** based on styrylpyridyl and benzofuran moieties, and ^{99m}Tc labeled coordination compounds [^{99m}Tc]138 and [^{99m}Tc]139, designed for SPECT imaging of Aβ plaques.

Molavipordanjani et al. reported two novel radiolabeled 2-arylimidazo[2,1-b]benzothiazoles **143** and **144** [95] (Figure 33). The affinity of the coordination compounds for $A\beta_{1-42}$ aggregates was evaluated, and both radiolabeled complexes showed a significant $A\beta$ binding. Tissue staining and autoradiography with Congo Red as a control proved an ability of the obtained complexes **143** and **144** to bind to $A\beta$ plaques in the brain sections of the rat AD model. Biodistribution studies in normal BALB/C mice showed an initial brain uptake of 0.78% and 0.86% ID/g respectively, for **143** and **144** in normal mice, followed by a nearly complete washout within an hour.

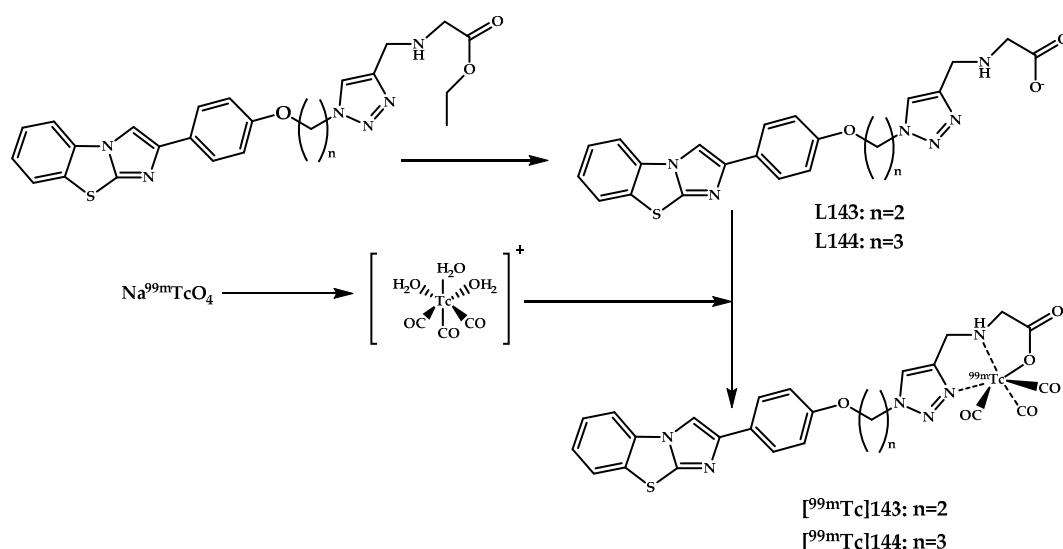


Figure 33. Radiolabeled 2-arylimidazo[2,1-b]benzothiazoles **143** and **144**, designed for SPECT imaging of $A\beta$ plaques.

Sagnou et al. reported synthesis of three novel ^{99m}Tc complexes [^{99m}Tc]**145**–[^{99m}Tc]**147** and their corresponding Re analogues **145**–**147**, in which the phenyl ring of the classical $A\beta$ -binding structures 2-phenylbenzothiazole or 2-phenylbenzimidazole is replaced by cyclopentadienyl tricarbonyl [$Cp^{99m}Tc(CO)_3$] [96] (Figure 34).

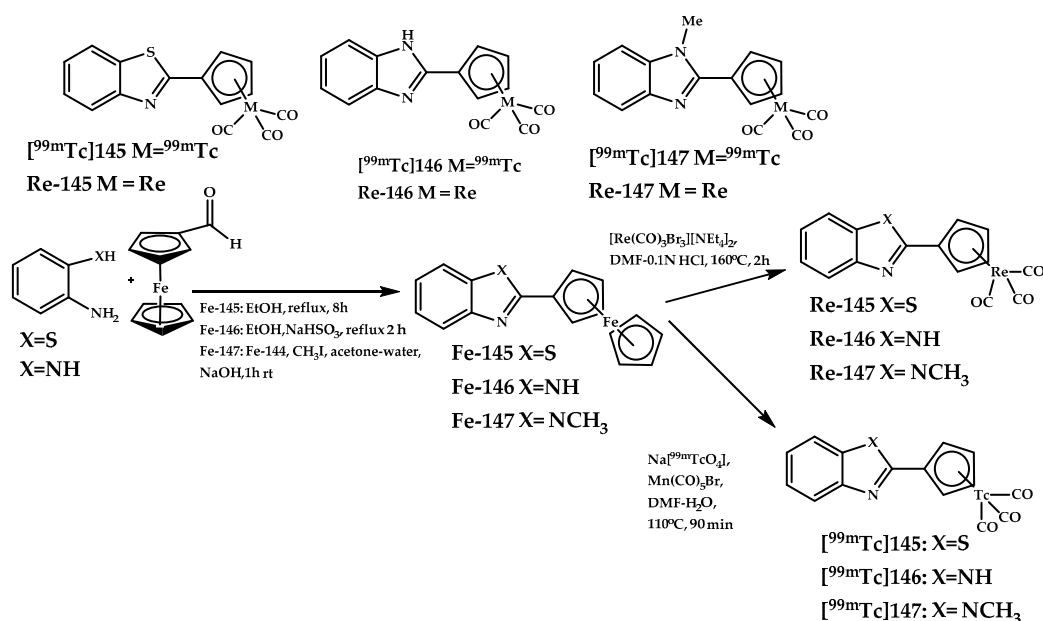


Figure 34. ^{99m}Tc complexes [^{99m}Tc]**145**–[^{99m}Tc]**147** and their corresponding Re analogues **145**–**147** designed for SPECT imaging of $A\beta$ plaques.

The affinity of complexes **145–147** for A β plaques was evaluated with confocal microscopy on human AD brain sections. All three complexes bind selectively to the A β plaques. Competition binding assays between the stable Re complexes **145–147** and their radioactive ^{99m}Tc counterparts [^{99m}Tc]**145**–[^{99m}Tc]**147** showed K_i values of 65.8 ± 21.3 , 7.0 ± 2.9 , and 5.7 ± 2.9 nM. Biodistribution experiments showed brain uptake of [^{99m}Tc]**145** ($7.94 \pm 1.46\%$) comparable to that of ^{18}F -florbetapir (7.33% ID/g at 2 min), fast blood clearance, and lack of retention in brain tissue.

Biodistribution of [^{99m}Tc]**145** in 5xFAD Tg-mice showed AD brain accumulation of 3.90 ± 0.19 for Tg-mice and 2.68 ± 0.06 for wild-type mice (15 min post-injection). The Re complexes **145–147** also showed an anti-amyloid therapeutic potential.

Jokar et al. designed a ^{99m}Tc agent **148** with a lipophilic peptide scaffold, ^{99m}Tc -Cp-GABA-D-(FPLIAIMA)-NH $_2$ [**97**] (Figure 35).

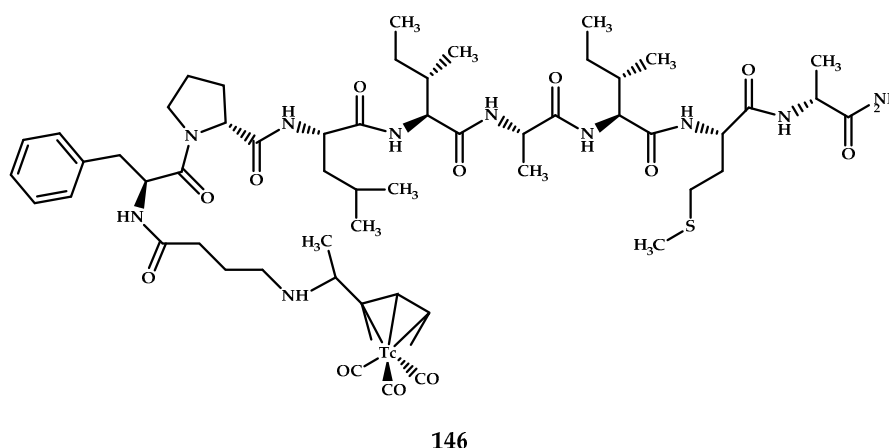


Figure 35. ^{99m}Tc -Cp-GABA-D-(FPLIAIMA)-NH $_2$ **148** based on an A β -affinitive peptide scaffold, designed for SPECT imaging of A β plaques.

Binding affinity studies were carried out on A β aggregation, and the respective observed values of K_d and B_{max} were 20.22 ± 7.26 μM and $201,700 \pm 8750.89$ bound molecules/plaque. In vitro autoradiography studies, scintigraphy, and fluorescence staining were performed on the brain sections of AD and normal rats and also on brain sections of AD, normal, and schizophrenia patients for better confirmation. The radiopeptide displayed a good binding affinity for the A β plaques on brain sections of AD rats and a significant binding affinity for A β plaques in human brain sections. Brain uptake in AD and normal rats was respectively 0.38% and 0.35% , and brain uptake of radiopeptide on AD brain increased 2 min post-injection and slowly dropped at 30 min, as compared with normal ones. Biodistribution studies in the presence of a p-glycoprotein (PgP) blocker and SPECT/CT imaging studies were also performed following intravenous administration of the probe. The analyzed images showed significant radioactivity uptake in the AD brains compared with uptake in normal rats.

5. Conclusions

Among various strategies utilized to obtain copper-based AD imaging agents, compound **1** with a low molecular mass and ATSM chelating moiety demonstrated the highest level of brain uptake at 2 min post-injection. We note that modification of the ATSM moiety with polyamine led to a significant increase in brain uptake. Other Cu-chelating fragments such as DOTA lead to a decrease in brain uptake compared with Cu-ATSM-based complexes.

Gd/Ga complexes designed for MRI and PET imaging of A β showed good in vitro activity, but when tested in vivo, those compounds showed little to no BBB penetration, which can result from the presence of rigid DOTA/DO3A, etc., scaffolds used to chelate Gd/Ga. The most potent compound

71 demonstrated a brain uptake of 1.24% ID/g at 2 min post-injection despite a MW \approx 1000, which is far beyond the optimal mass for BBB penetration.

Some of the ^{99m}Tc -based coordination compounds demonstrated promising in vitro and in vivo activity. The most potent complexes for SPECT imaging were compounds **145–147** with piano stool moieties coupled with A β -binding benzothiazole scaffolds, with **145** showing a brain uptake of 7.94% at 2 min post-injection. When rigid chelating structures, long linkers, and heavy A β -binding fragments are used, the BBB penetrability of the resulting coordination compounds decreases dramatically, as shown for **92–95** and **107–132**.

Metal-based imaging agents for AD allow noninvasive imaging of A β plaques, a crucial procedure for successful AD diagnosis and therapy. There is a strong need for new efficient AD imaging probes, and this area of research is therefore thriving. The radioisotopes ^{64}Cu , ^{68}Ga , and ^{99m}Tc are promising and can be obtained either by cyclotrons or by radioisotope generators. They also have half-lives much longer than do ^{18}F and ^{11}C , which are currently used for imaging. Radioactive metal isotopes can be introduced at the last step of synthesizing an imaging agent, which reduces the potential activity loss.

Among the vast variety of compounds considered in this review, the most promising results were shown by Cu^{2+} -based coordination compounds **1** and **11** for PET imaging, Gd^{3+} -based coordination compound **40** for MRI, and ^{99m}Tc -based coordination compound **145** for SPECT imaging, demonstrating the best A β -binding affinity and brain uptake at 2 min post-injection while being light-weight complexes with small A β -binding fragments.

Author Contributions: Conceptualization, O.K. and D.S.; Writing—Original Draft Preparation, O.K. and D.S.; Writing—Review & Editing, O.K., D.S., A.Z., K.P., P.G., A.E.; Visualization, D.S., A.Z., K.P.; Supervision, P.G., A.E.; Project Administration, E.B. A.M.; Funding Acquisition, P.G., A.E., A.M. All authors have read and agreed to the published version of the manuscript.

Funding: This research was funded by the Ministry of Education and Science of the Russian Federation implemented by governmental decree No. 211 dated 16 March 2013, and by the Russian Science Foundation, Grant No. 20-14-00312.

Conflicts of Interest: The authors declare no conflict of interest.

Abbreviations

| | |
|------------------------|--|
| ^{125}I JIMPY | (^{125}I)6-iodo-2-(40-dimethylamino)-phenyl-imidazo [1,2-a]pyridine) |
| ICP-MS | inductively coupled plasma mass spectrometry |
| ^{18}F FDDNP | (1,1-dicyanopropen-2-yl)-6-(2-[^{18}F]-fluoroethyl)-methylamino-naphthalene |
| SPECT | single-photon emission computed tomography |
| PET | positron emission tomography |
| MRI | magnetic resonance imaging |
| AD | Alzheimer's disease |
| BBB | Blood-brain barrier |
| CAA | cerebral amyloid angiopathy |
| PgP | P-glycoprotein |
| TEM | transmission electron microscopy |
| Tg-mice | transgenic mice |
| ThT | Thioflavin-T |
| DOTA | 1,4,7,10-tetraazacyclododecane-1,4,7,10-tetraacetic acid |
| DO3A | 1,4,7,10-tetraazacyclododecane-1,4,7-triacetic acid |
| PCTA | 3,6,9,15-tetraaza bicyclo[9.3.1]-pentadeca1(15),11,13-triene-3,6,9-triacetic acid |
| HBED-CC | N,N'-bis[2-hydroxy-5-(carboxyethyl)benzyl]ethylenediamine-N,N'-diacetic acid |
| NODAGA | 1,4,7-triazacyclononane,1-glutaric acid-4,7-acetic acid |
| AAZTA | 1,4-bis(carboxymethyl)-6-[bis(carboxymethyl)]amino-6-methylperhydro-1,4-diazepine |
| BAT- | Bis-amino bis-thiol |
| MAMA | Monoamine-monoamide dithiols |
| IC ₅₀ | The half maximal inhibitory concentration |
| MTT | (3-(4,5-dimethylthiazol-2-yl)-2,5-diphenyltetrazolium bromide |
| PIB | 2-(4'-[^{11}C]methylaminophenyl)-6-hydroxybenzothiazole |

References

1. Penke, B.; Szűcs, M.; Bogár, F. Oligomerization and Conformational Change Turn Monomeric β -Amyloid and Tau Proteins Toxic: Their Role in Alzheimer's Pathogenesis. *Molecules* **2020**, *25*, 1659. [[CrossRef](#)]
2. Chen, G.-F.; Xu, T.-H.; Yan, Y.; Zhou, Y.-R.; Jiang, Y.; Melcher, K.; Xu, H.E. Amyloid beta: Structure, biology and structure-based therapeutic development. *Acta Pharmacol. Sin.* **2017**, *38*, 1205–1235. [[CrossRef](#)]
3. Savelieff, M.G.; Lee, S.; Liu, Y.; Lim, M.H. Untangling Amyloid- β , Tau, and Metals in Alzheimer's Disease. *ACS Chem. Biol.* **2013**, *8*, 856–865. [[CrossRef](#)]
4. LaFerla, F.M.; Green, K.N.; Oddo, S. Intracellular amyloid- β in Alzheimer's disease. *Nat. Rev. Neurosci.* **2007**, *8*, 499–509. [[CrossRef](#)]
5. Verhoeff, N.P.; Wilson, A.A.; Takeshita, S.; Trop, L.; Hussey, D.; Singh, K.; Kung, H.F.; Kung, M.P.; Houle, S. In-vivo imaging of Alzheimer disease beta-amyloid with $[^{11}\text{C}]\text{SB-13}$ PET. *Am. J. Geriatr. Psychiatry* **2004**, *12*, 584–595.
6. Rowe, C.C.; Villemagne, V.L. Brain Amyloid Imaging. *J. Nucl. Med. Technol.* **2013**, *41*, 11–18. [[CrossRef](#)]
7. Roe, C.M.; Fagan, A.M.; Grant, E.A.; Hassenstab, J.; Moulder, K.L.; Dreyfus, D.M.; Sutphen, C.L.; Benzinger, T.L.S.; Mintun, M.A.; Holtzman, D.M.; et al. Amyloid imaging and CSF biomarkers in predicting cognitive impairment up to 7.5 years later. *Neurology* **2013**, *80*, 1784–1791. [[CrossRef](#)]
8. Therriault, J.; Benedet, A.; Pascoal, T.A.; Savard, M.; Ashton, N.; Chamoun, M.; Tissot, C.; Lussier, F.; Kang, M.S.P.; Bezgin, G.; et al. Determining Amyloid- β positivity using $[^{18}\text{F}]\text{AZD}_{4694}$ PET imaging. *J. Nucl. Med.* **2020**, *120*, 245209.
9. Chang, Y.; Li, C.; Yang, H.; Wu, Y.; Xu, B.; Zhang, J.; Wang, R. ^{18}F -Florbetaben Amyloid PET Imaging: A Chinese Study in Cognitive Normal Controls, Mild Cognitive Impairment, and Alzheimer's Disease Patients. *Front. Neurosci.* **2020**, *14*, 745. [[CrossRef](#)]
10. Cohen, A.D.; Rabinovici, G.D.; Mathis, C.A.; Jagust, W.J.; Klunk, W.E.; Ikonovic, M.D. Using Pittsburgh Compound B for In Vivo PET Imaging of Fibrillar Amyloid-Beta. *Adv. Pharmacol.* **2012**, *64*, 27–81.
11. Carotenuto, A.; Giordano, B.; Dervenoulas, G.; Wilson, H.; Veronese, M.; Chappell, Z.; Polychronis, S.; Pagano, G.; Mackewn, J.; Turkheimer, F.E.; et al. $[^{18}\text{F}]$ Florbetapir PET/MR imaging to assess demyelination in multiple sclerosis. *Eur. J. Nucl. Med. Mol. Imaging* **2020**, *47*, 366–378. [[CrossRef](#)] [[PubMed](#)]
12. Chételat, G.; Arbizu, J.; Barthel, H.; Garibotto, V.; Law, I.; Morbelli, S.; van de Giessen, E.; Agosta, F.; Barkhof, F.; Brooks, D.J.; et al. Amyloid-PET and ^{18}F -FDG-PET in the diagnostic investigation of Alzheimer's disease and other dementias. *Lancet Neurol.* **2020**, *19*, 951–962. [[CrossRef](#)]
13. Moynier, F.; Creech, J.; Dallas, J.; Le Borgne, M. Serum and brain natural copper stable isotopes in a mice model of Alzheimer's disease. *Sci. Rep.* **2019**, *9*, 1–7. [[CrossRef](#)]
14. Lau, J.; Rousseau, E.; Kwon, D.; Lin, K.-S.; Bénard, F.; Chen, X. Insight into the Development of PET Radiopharmaceuticals for Oncology. *Cancers* **2020**, *12*, 1312. [[CrossRef](#)] [[PubMed](#)]
15. Meisenheimer, M.; Saenko, Y.; Eppard, E. Gallium-68: Radiolabeling of Radiopharmaceuticals for PET Imaging—A Lot to Consider. *Med Isot.* **2019**. [[CrossRef](#)]
16. Romero, E.; Martínez, A.; Oteo, M.; Ibañez, M.; Santos, M.; Morcillo, M.Á. Development and long-term evaluation of a new $^{68}\text{Ge}/^{68}\text{Ga}$ generator based on nano-SnO₂ for PET imaging. *Sci. Rep.* **2020**, *10*, 12756. [[CrossRef](#)]
17. Dash, A.; Chakravarty, R. Radionuclide generators: The prospect of availing PET radiotracers to meet current clinical needs and future research demands. *Am. J. Nucl. Med. Mol. Imaging* **2019**, *9*, 30–66.
18. Boschi, A.; Uccelli, L.; Martini, P. A Picture of Modern Tc-99m Radiopharmaceuticals: Production, Chemistry, and Applications in Molecular Imaging. *Appl. Sci.* **2019**, *9*, 2526. [[CrossRef](#)]
19. Wang, C.; Wang, X.; Chan, H.; Chan, H.-N.; Liu, G.; Wang, Z.; Li, H.; Li, H.-W.; Wong, M.S. Amyloid- β Oligomer-Targeted Gadolinium-Based NIR/MR Dual-Modal Theranostic Nanoprobe for Alzheimer's Disease. *Adv. Funct. Mater.* **2020**, *30*, 1909529. [[CrossRef](#)]
20. Abbott, N.J.; Patabendige, A.A.K.; Dolman, D.E.M.; Yusof, S.R.; Begley, D.J. Structure and function of the blood-brain barrier. *Neurobiol. Dis.* **2010**, *37*, 13–25. [[CrossRef](#)]
21. Daneman, R.; Prat, A. The Blood-Brain Barrier. *Cold Spring Harb. Perspect. Biol.* **2015**, *7*, a020412. [[CrossRef](#)]
22. He, Q.; Liu, J.; Liang, J.; Liu, X.; Li, W.; Liu, Z.; Ding, Z.; Tuo, D. Towards improvements for penetrating the blood-brain barrier—Recent progress from a material and pharmaceutical perspective. *Cells* **2018**, *7*, 24. [[CrossRef](#)]

23. Rautio, J.; Laine, K.; Gynther, M.; Savolainen, J. Prodrug approaches for CNS delivery. *AAPS J.* **2008**, *10*, 92–102. [[CrossRef](#)]
24. Aryal, M.; Arvanitis, C.D.; Alexander, P.M.; McDannold, N. Ultrasound-mediated blood-brain barrier disruption for targeted drug delivery in the central nervous system. *Adv. Drug Deliv. Rev.* **2014**, *72*, 94–109. [[CrossRef](#)]
25. Polat, B.E.; Blankschtein, D.; Langer, R. Low-frequency sonophoresis: Application to the transdermal delivery of macromolecules and hydrophilic drugs. *Expert Opin. Drug Deliv.* **2010**, *7*, 1415–1432. [[CrossRef](#)]
26. Wood, I.S.; Trayhurn, P. Glucose transporters (GLUT and SGLT): Expanded families of sugar transport proteins. *Br. J. Nutr.* **2007**, *89*, 3–9. [[CrossRef](#)] [[PubMed](#)]
27. Oddo, A.; Peng, B.; Tong, Z.; Wei, Y.; Tong, W.Y.; Thissen, H.; Voelcker, N.H. Advances in Microfluidic Blood-Brain Barrier (BBB) Models. *Trends Biotechnol.* **2019**, *12*, 1295–1314. [[CrossRef](#)]
28. Di Lullo, E.; Kriegstein, A.R. The use of brain organoids to investigate neural development and disease. *Nat. Rev. Neurosci.* **2017**, *18*, 573–584. [[CrossRef](#)]
29. Salman, M.M.; Marsh, G.; Kusters, I.; Delincé, M.; Di Caprio, G.; Upadhyayula, S.; de Nola, G.; Hunt, R.; Ohashi, K.G.; Gray, T.; et al. Design and Validation of a Human Brain Endothelial Microvessel-on-a-Chip Open Microfluidic Model Enabling Advanced Optical Imaging. *Front. Bioeng. Biotechnol.* **2020**, *8*, 1077. [[CrossRef](#)]
30. Mensch, J.; Oyarzabal, J.; Mackie, C.; Augustijns, P. *In vivo*, *in vitro* and *in silico* methods for small molecule transfer across the BBB. *J. Pharm. Sci.* **2009**, *98*, 4429–4468. [[CrossRef](#)]
31. Van de Waterbeemd, H.; Camenisch, G.; Folkers, G.; Chretien, J.R.; Raevsky, O.A. Estimation of blood-brain barrier crossing of drugs using molecular size and shape, and H-bonding descriptors. *J. Drug Target* **1998**, *6*, 151–165. [[CrossRef](#)]
32. Sedgwick, A.C.; Brewster II, J.T.; Harvey, P.; Iovan, D.A.; Smith, G.; He, X.-P.; Tian, H.; Sessler, J.L.; James, T.D. Metal-based imaging agents: Progress towards interrogating neurodegenerative disease. *Chem. Soc. Rev.* **2020**, *49*, 2886–2915. [[CrossRef](#)]
33. Gomes, L.M.F.; Bataglioli, J.C.; Storr, T. Metal complexes that bind to the amyloid- β peptide of relevance to Alzheimer's disease. *Coord. Chem. Rev.* **2020**, *412*, 213255. [[CrossRef](#)]
34. Liu, H.; Qu, Y.; Wang, X. Amyloid β -targeted metal complexes for potential applications in Alzheimer's disease. *Future Med. Chem.* **2018**, *10*, 679–701. [[CrossRef](#)]
35. Daghighian, F.; Sumida, R.; Phelps, M.E. PET Imaging: An Overview and Instrumentation. *J. Nucl. Med. Technol.* **1990**, *18*, 5–15.
36. Sin, I.; Kang, C.S.; Bandara, N.; Sun, X.; Zhong, Y.L.; Rogers, B.E.; Chong, H.S. Novel hexadentate and pentadentate chelators for ^{64}Cu -based targeted PET imaging. *Bioorg. Med. Chem.* **2014**, *22*, 2553–2562. [[CrossRef](#)]
37. Kim, D.-K.; Song, J.-W.; Park, J.-D.; Choi, B.-S. Copper induces the accumulation of amyloid-beta in the brain. *Mol. Cell. Toxicol.* **2013**, *9*, 57–66. [[CrossRef](#)]
38. Liu, T.; Karlsen, M.; Karlberg, A.M.; Redalen, K.R. Hypoxia imaging and theranostic potential of [^{64}Cu][Cu(ATSM)] and ionic Cu(II) salts: A review of current evidence and discussion of the retention mechanisms. *Eur. J. Nucl. Med. Mol. Imaging* **2020**, *10*, 33. [[CrossRef](#)]
39. Sharma, A.K.; Schultz, J.W.; Prior, J.T.; Rath, N.P.; Mirica, L.M. Coordination Chemistry of Bifunctional Chemical Agents Designed for Applications in ^{64}Cu PET Imaging for Alzheimer's Disease. *Inorg. Chem.* **2017**, *56*, 13801–13814. [[CrossRef](#)]
40. Lim, S.; Paterson, B.M.; Fodero-Tavoletti, M.T.; O'Keefe, G.J.; Cappai, R.; Barmham, K.J.; Villemagne, V.L.; Donnelly, P.S. A copper radiopharmaceutical for diagnostic imaging of Alzheimer's disease: A bis (thiosemicarbazonato)copper(II) complex that binds to amyloid- β plaques. *Chem. Commun.* **2010**, *46*, 5437–5439. [[CrossRef](#)]
41. Hickey, J.L.; Lim, S.; Hayne, D.J.; Paterson, B.M.; White, J.M.; Villemagne, V.L.; Roselt, P.; Binns, D.; Cullinane, C.; Jeffery, C.M.; et al. Diagnostic Imaging Agents for Alzheimer's Disease: Copper Radiopharmaceuticals that Target A β Plaques. *J. Am. Chem. Soc.* **2013**, *135*, 16120–16132. [[CrossRef](#)] [[PubMed](#)]
42. McInnes, L.E.; Noor, A.; Kysenius, K.; Cullinane, C.; Roselt, P.; McLean, C.A.; Chiu, F.C.K.; Powell, A.K.; Crouch, P.J.; White, J.M.; et al. Potential Diagnostic Imaging of Alzheimer's Disease with Copper-64 Complexes That Bind to Amyloid- β Plaques. *Inorg. Chem.* **2019**, *58*, 3382–3395. [[CrossRef](#)] [[PubMed](#)]

43. McInnes, L.E.; Noor, A.; Roselt, P.D.; McLean, C.A.; White, J.M.; Donnelly, P.S. A Copper Complex of a Thiosemicarbazone-Pyridylhydrazone Ligand Containing a Vinylpyridine Functional Group as a Potential Imaging Agent for Amyloid- β Plaques. *Aust. J. Chem.* **2019**, *72*, 827. [[CrossRef](#)]
44. Noor, A.; Hayne, D.J.; Lim, S.; Van Zuylenkom, J.K.; Cullinane, C.; Roselt, P.D.; McLean, C.A.; White, J.M.; Donnelly, P.S. Copper Bis(thiosemicarbazonato)-stilbenyl Complexes That Bind to Amyloid- β Plaques. *Inorg. Chem.* **2020**, *59*, 11658–11669. [[CrossRef](#)] [[PubMed](#)]
45. Paterson, B.M.; Cullinane, C.; Crouch, P.J.; White, A.R.; Barnham, K.J.; Roselt, P.D.; Noonan, W.; Binns, D.; Hicks, R.J.; Donnelly, P.S. Modification of Biodistribution and Brain Uptake of Copper Bis(thiosemicarbazonato) Complexes by the Incorporation of Amine and Polyamine Functional Groups. *Inorg. Chem.* **2019**, *58*, 4540–4552. [[CrossRef](#)]
46. Watanabe, H.; Kawasaki, A.; Sano, K.; Ono, M.; Saji, H. Synthesis and evaluation of copper-64 labeled benzofuran derivatives targeting β -amyloid aggregates. *Bioorg. Med. Chem.* **2016**, *24*, 3618–3623. [[CrossRef](#)]
47. Bandara, N.; Sharma, A.K.; Krieger, S.; Schultz, J.W.; Han, B.H.; Rogers, B.E.; Mirica, L.M. Evaluation of ^{64}Cu -Based Radiopharmaceuticals that Target A β Peptide Aggregates as Diagnostic Tools for Alzheimer's Disease. *J. Am. Chem. Soc.* **2017**, *139*, 12550–12558. [[CrossRef](#)]
48. Huang, Y.; Cho, H.-J.; Bandara, N.; Sun, L.; Tran, D.; Rogers, B.E.; Mirica, L.M. Metal-chelating benzothiazole multifunctional compounds for the modulation and ^{64}Cu PET imaging of A β aggregation. *Chem. Sci.* **2020**, *11*, 7789–7799. [[CrossRef](#)]
49. Sharma, A.K.; Pavlova, S.T.; Kim, J.; Finkelstein, D.; Hawco, N.J.; Rath, N.P.; Kim, J.; Mirica, L.M. Bifunctional Compounds for Controlling Metal-Mediated Aggregation of the A β_{42} Peptide. *J. Am. Chem. Soc.* **2012**, *134*, 6625–6636. [[CrossRef](#)]
50. Sharma, A.K.; Kim, J.; Prior, J.T.; Hawco, N.J.; Rath, N.P.; Kim, J.; Mirica, L.M. Small Bifunctional Chelators That Do Not Disaggregate Amyloid β Fibrils Exhibit Reduced Cellular Toxicity. *Inorg. Chem.* **2014**, *53*, 11367–11376. [[CrossRef](#)]
51. Banerjee, S.R.; Pomper, M.G. Clinical applications of Gallium-68. *Appl. Radiat. Isot.* **2013**, *76*, 2–13. [[CrossRef](#)] [[PubMed](#)]
52. Moerlein, S.M.; Welch, M.J. The chemistry of gallium and indium as related to radiopharmaceutical production. *Int. J. Nucl. Med. Biol.* **1981**, *8*, 277–287. [[CrossRef](#)]
53. Zhou, Z.; Lu, Z.-R. Gadolinium-based contrast agents for magnetic resonance cancer imaging. *Wiley Interdiscip. Rev. Nanomed. Nanobiotechnol.* **2013**, *5*, 1–18. [[CrossRef](#)] [[PubMed](#)]
54. Caravan, P.; Ellison, J.J.; McMurry, T.J.; Lauffer, R.B. Gadolinium(III) Chelates as MRI Contrast Agents: Structure, Dynamics, and Applications. *Chem. Rev.* **1999**, *99*, 2293–2352. [[CrossRef](#)]
55. Martins, A.F.; Morfin, J.-F.; Kubíčková, A.; Kubíček, V.; Buron, F.; Suzenet, F.; Salerno, M.; Lazar, A.N.; Duyckaerts, C.; Arlicot, N.; et al. PiB-Conjugated, Metal-Based Imaging Probes: Multimodal Approaches for the Visualization of β -Amyloid Plaques. *ACS Med. Chem. Lett.* **2013**, *4*, 436–440. [[CrossRef](#)]
56. Martins, A.F.; Morfin, J.-F.; Geraldès, C.F.G.C.; Tóth, É. Gd^{3+} complexes conjugated to Pittsburgh compound B: Potential MRI markers of β -amyloid plaques. *J. Biol. Inorg. Chem.* **2014**, *19*, 281–295. [[CrossRef](#)]
57. Bort, G.; Catoen, S.; Borderies, H.; Keksi, A.; Ballet, S.; Louin, G.; Port, M.; Ferroud, C. Gadolinium-based contrast agents targeted to amyloid aggregates for the early diagnosis of Alzheimer's disease by MRI. *Eur. J. Med. Chem.* **2014**, *87*, 843–861. [[CrossRef](#)]
58. Watanabe, H.; Ono, M.; Iikuni, S.; Yoshimura, M.; Matsumura, K.; Kimura, H.; Saji, H. A ^{68}Ga complex based on benzofuran scaffold for the detection of β -amyloid plaques. *Bioorg. Med. Chem. Lett.* **2014**, *24*, 4834–4837. [[CrossRef](#)]
59. Cressier, D.; Dhilly, M.; Cao Pham, T.T.; Fillesoye, F.; Gourand, F.; Maïza, A.; Martins, A.F.; Morfin, J.-F.; Geraldès, C.F.G.C.; Tóth, É.; et al. Gallium-68 Complexes Conjugated to Pittsburgh Compound B: Radiolabeling and Biological Evaluation. *Mol. Imaging Biol.* **2016**, *18*, 334–343. [[CrossRef](#)]
60. Zha, Z.; Song, J.; Choi, S.R.; Wu, Z.; Ploessl, K.; Smith, M.; Kung, H. ^{68}Ga -Bivalent Polypegylated Styrylpyridine Conjugates for Imaging A β Plaques in Cerebral Amyloid Angiopathy. *Bioconjug. Chem.* **2016**, *27*, 1314–1323. [[CrossRef](#)]
61. Chauhan, K.; Datta, A.; Adhikari, A.; Chuttani, K.; Singh, A.K.; Mishra, A.K. ^{68}Ga based probe for Alzheimer's disease: Synthesis and preclinical evaluation of homodimeric chalcone in β -amyloid imaging. *Org. Biomol. Chem.* **2014**, *12*, 7328. [[CrossRef](#)] [[PubMed](#)]

62. Asti, M.; Ferrar, E.; Croci, S.; Atti, G.; Rubagotti, S.; Iori, M.; Capponi, P.C.; Zerbini, A.; Saladini, M.; Versari, A. Synthesis and Characterization of ⁶⁸Ga-Labeled Curcumin and Curcuminoid Complexes as Potential Radiotracers for Imaging of Cancer and Alzheimer's Disease. *Inorg. Chem.* **2014**, *53*, 4922–4933. [[CrossRef](#)] [[PubMed](#)]
63. Rubagotti, S.; Croci, S.; Ferrari, E.; Iori, M.; Capponi, P.C.; Lorenzini, L.; Calzà, L.; Versari, A.; Asti, M. Affinity of (nat/68)Ga-Labelled Curcumin and Curcuminoid Complexes for β -Amyloid Plaques: Towards the Development of New Metal-Curcumin Based Radiotracers. *Int. J. Mol. Sci.* **2016**, *17*, 1480. [[CrossRef](#)] [[PubMed](#)]
64. Lange, J.L.; Hayne, D.J.; Roselt, P.; McLean, C.A.; White, J.M.; Donnelly, P.S. A gallium(III) Schiff base-curcumin complex that binds to amyloid- β plaques. *J. Inorg. Biochem.* **2016**, *162*, 274–279. [[CrossRef](#)]
65. Orteca, G.; Sinnes, J.-P.; Rubagotti, S.; Iori, M.; Capponi, P.C.; Piel, M.; Rösch, F.; Ferrari, E.; Asti, M. Gallium-68 and scandium-44 labelled radiotracers based on curcumin structure linked to bifunctional chelators: Synthesis and characterization of potential PET radiotracers. *J. Inorg. Biochem.* **2020**, *204*, 110954.
66. Gniazdowska, E.; Koźmiński, P.; Halik, P.; Bajda, M.; Czarnecka, K.; Mikiciuk-Olasik, E.; Mastowska, K.; Rogulski, Z.; Cheda, Ł.; Kilian, K.; et al. Synthesis, physicochemical and biological evaluation of tacrine derivative labeled with technetium-99m and gallium-68 as a prospective diagnostic tool for early diagnosis of Alzheimer's disease. *Bioorg. Chem.* **2019**, *91*, 103136. [[CrossRef](#)]
67. Singh, S.; Khar, A. Biological Effects of Curcumin and Its Role in Cancer Chemoprevention and Therapy. *AntiCancer Agents Med. Chem.* **2006**, *6*, 933–946. [[CrossRef](#)]
68. Bartik, L.; Whitfield, G.K.; Kaczmarek, M.; Lowmiller, C.L.; Moffet, E.W.; Furnick, J.K.; Hernandez, Z.; Haussler, C.A.; Haussler, M.R.; Jurutka, P.W. Curcumin: A novel nutritionally derived ligand of the vitamin D receptor with implications for colon cancer chemoprevention. *J. Nutr. Biochem.* **2010**, *21*, 1153–1161. [[CrossRef](#)]
69. Chen, M.; Du, Z.Y.; Zheng, X.; Li, D.L.; Zhou, R.P.; Zhang, K. Use of curcumin in diagnosis, prevention, and treatment of Alzheimer's disease. *Neural Regen. Res.* **2018**, *13*, 742–752.
70. Sidiqi, A.; Wahl, D.; Lee, S.; Ma, D.; To, E.; Cui, J.; To, E.; Beg, M.F.; Sarunic, M.; Matsubara, J.A. In vivo Retinal Fluorescence Imaging with Curcumin in an Alzheimer Mice Model. *Front. Neurosci.* **2020**, *14*, 713. [[CrossRef](#)]
71. McCrate, O.A.; Zhou, X.; Cegelski, L. Curcumin as an amyloid-indicator dye in *E. coli*. *Chem. Commun.* **2013**, *49*, 4193–4195. [[CrossRef](#)] [[PubMed](#)]
72. Thapa, A.; Jett, S.D.; Chi, E.Y. Curcumin Attenuates Amyloid- β Aggregate Toxicity and Modulates Amyloid- β Aggregation Pathway. *ACS Chem. Neurosci.* **2016**, *7*, 56–68. [[CrossRef](#)] [[PubMed](#)]
73. Teoh, C.L.; Su, D.; Sahu, S.; Yun, S.-W.; Drummond, E.; Prelli, F.; Lim, S.; Cho, S.; Ham, S.; Wisniewski, T.; et al. Chemical Fluorescent Probe for Detection of A β Oligomers. *J. Am. Chem. Soc.* **2015**, *137*, 13503–13509. [[CrossRef](#)] [[PubMed](#)]
74. Ono, K.; Hasegawa, K.; Naiki, H.; Yamada, M.J. Curcumin has potent anti-amyloidogenic effects for Alzheimer's β -amyloid fibrils in vitro. *Neurosci. Res.* **2004**, *75*, 742–750. [[CrossRef](#)] [[PubMed](#)]
75. Yang, J.; Cheng, R.; Fu, H.; Yang, J.; Kumar, M.; Lu, J.; Xu, Y.; Liang, S.H.; Cui, M.; Ran, C. Half-curcumin analogues as PET imaging probes for amyloid beta species. *Chem. Comm.* **2019**, *55*, 3630–3633. [[CrossRef](#)] [[PubMed](#)]
76. Sherin, S.; Balachandran, S.; Abraham, A. Curcumin incorporated titanium dioxide nanoparticles as MRI contrasting agent for early diagnosis of atherosclerosis- rat model. *Vet. Anim. Sci.* **2020**, *10*, 100090. [[CrossRef](#)] [[PubMed](#)]
77. Ono, M.; Haratake, M.; Mori, H.; Nakayama, M. Novel chalcones as probes for in vivo imaging of beta-amyloid plaques in Alzheimer's brains. *Bioorg. Med. Chem.* **2007**, *15*, 6802–6809. [[CrossRef](#)]
78. Yang, F.; Lim, G.P.; Begum, A.N.; Ubeda, O.J.; Simmons, M.R.; Ambegaokar, S.S.; Chen, P.P.; Kaye, R.; Glabe, C.G.; Frautschy, S.A.; et al. Curcumin Inhibits Formation of Amyloid β Oligomers and Fibrils, Binds Plaques, and Reduces Amyloid in Vivo. *J. Biol. Chem.* **2005**, *280*, 5892–5901. [[CrossRef](#)]
79. Jeyarasasingam, G.; Yelushvili, M.; Quik, M. Tacrine, a reversible acetylcholinesterase inhibitor, induces myopathy. *NeuroReport* **2000**, *11*, 1173–1176. [[CrossRef](#)]
80. Meszaros, L.K.; Dose, A.; Biagini, S.C.G.; Blower, P.J. Synthesis and evaluation of analogues of HYNIC as bifunctional chelators for technetium. *Dalton Trans.* **2011**, *40*, 6260–6267. [[CrossRef](#)]

81. Fissers, J.; Waldron, A.-M.; De Vijlder, T.; Van Broeck, B.; Pemberton, D.J.; Mercken, M.; Van Der Veken, P.; Joossens, J.; Augustyns, K.; Dedeurwaerdere, S.; et al. Synthesis and Evaluation of a Zr-89-Labeled Monoclonal Antibody for Immuno-PET Imaging of Amyloid- β Deposition in the Brain. *Mol. Imaging Biol.* **2016**, *18*, 598–605. [[PubMed](#)]
82. Jia, J.; Cui, M.; Dai, J.; Wang, X.; Ding, Y.-S.; Jia, H.; Liu, B. ^{99m}Tc -labeled benzothiazole and stilbene derivatives as imaging agents for A β plaques in cerebral amyloid angiopathy. *Med. Chem. Comm.* **2014**, *5*, 153–158. [[CrossRef](#)]
83. Li, Z.; Cui, M.; Dai, J.; Wang, X.; Yu, P.; Yang, Y.; Jia, J.; Fu, H.; Ono, M.; Jia, H.; et al. Novel Cyclopentadienyl Tricarbonyl Complexes of ^{99m}Tc Mimicking Chalcone as Potential Single-Photon Emission Computed Tomography Imaging Probes for β -Amyloid Plaques in Brain. *J. Med. Chem.* **2013**, *56*, 471–482. [[CrossRef](#)] [[PubMed](#)]
84. Yang, Y.; Cui, M.; Jin, B.; Wang, X.; Li, Z.; Yu, P.; Jia, J.; Fu, H.; Jia, H.; Liu, B. ^{99m}Tc -labeled dibenzylideneacetone derivatives as potential SPECT probes for in vivo imaging of β -amyloid plaque. *Eur. J. Med. Chem.* **2013**, *64*, 90–98. [[CrossRef](#)] [[PubMed](#)]
85. Iikuni, S.; Ono, M.; Watanabe, H.; Matsumura, K.; Yoshimura, M.; Harada, N.; Kimura, H.; Nakayama, M.; Saji, H. Enhancement of Binding Affinity for Amyloid Aggregates by Multivalent Interactions of ^{99m}Tc -Hydroxamamide Complexes. *Mol. Pharm.* **2014**, *11*, 1132–1139. [[CrossRef](#)]
86. Iikuni, S.; Ono, M.; Watanabe, H.; Matsumura, K.; Yoshimura, M.; Kimura, H.; Ishibashi-Ueda, H.; Okamoto, Y.; Ihara, M.; Saji, H. Imaging of Cerebral Amyloid Angiopathy with Bivalent ^{99m}Tc -Hydroxamamide Complexes. *Sci. Rep.* **2016**, *6*, 25990. [[CrossRef](#)]
87. Hayne, D.J.; North, A.J.; Fodero-Tavoletti, M.; White, J.M.; Hung, L.W.; Rigopoulos, A.; McLean, C.A.; Adlard, P.A.; Ackermann, U.; Tochon-Danguy, H.; et al. Rhenium and technetium complexes that bind to amyloid- β plaques. *Dalton Trans.* **2015**, *44*, 4933–4944. [[CrossRef](#)]
88. Wang, X.; Cui, M.; Jia, J.; Liu, B. ^{99m}Tc -labeled-2-arylbenzoxazole derivatives as potential A β imaging probes for single-photon emission computed tomography. *Eur. J. Med. Chem.* **2015**, *89*, 331–339. [[CrossRef](#)]
89. Jia, J.; Cui, M.; Dai, J.; Liu, B. $^{99m}\text{Tc}(\text{CO})_3$ -Labeled Benzothiazole Derivatives Preferentially Bind Cerebrovascular Amyloid: Potential Use as Imaging Agents for Cerebral Amyloid Angiopathy. *Mol. Pharm.* **2015**, *12*, 2937–2946. [[CrossRef](#)]
90. Zhang, X.; Yu, P.; Yang, Y.; Hou, Y.; Peng, C.; Liang, Z.; Lu, J.; Chen, B.; Dai, J.; Liu, B.; et al. ^{99m}Tc -Labeled 2-Arylbenzothiazoles: A β Imaging Probes with Favorable Brain Pharmacokinetics for Single-Photon Emission Computed Tomography. *Bioconj. Chem.* **2016**, *27*, 2493–2504. [[CrossRef](#)]
91. Hayne, D.J.; White, J.M.; McLean, C.A.; Villemagne, V.L.; Barnham, K.J.; Donnelly, P.S. Synthesis of Oxorhenium(V) and Oxotechnetium(V) Complexes That Bind to Amyloid- β Plaques. *Inorg. Chem.* **2016**, *55*, 7944–7953. [[CrossRef](#)] [[PubMed](#)]
92. Kiritsis, C.; Mavroidi, B.; Shegani, A.; Palamaris, L.; Loudos, G.; Sagnou, M.; Pirmettis, I.; Papadopoulos, M.; Pelecanou, M. 2-(4'-Aminophenyl)benzothiazole Labeled with ^{99m}Tc -Cyclopentadienyl for Imaging β -Amyloid Plaques. *ACS Med. Chem. Lett.* **2017**, *8*, 1089–1092. [[CrossRef](#)] [[PubMed](#)]
93. Iikuni, S.; Ono, M.; Tanimura, K.; Watanabe, H.; Yoshimura, M.; Saji, H. Synthesis and biological evaluation of novel technetium- 99m -labeled phenylquinoxaline derivatives as single photon emission computed tomography imaging probes targeting β -amyloid plaques in Alzheimer's disease. *RSC Adv.* **2017**, *7*, 20582–20590. [[CrossRef](#)]
94. Fletcher, S.P.; Noor, A.; Hickey, J.L.; McLean, C.A.; White, J.M.; Donnelly, P.S. Rhenium and technetium complexes of thioamide derivatives of pyridylhydrazine that bind to amyloid- β plaques. *J. Biol. Inorg. Chem.* **2018**, *23*, 1139–1151. [[CrossRef](#)] [[PubMed](#)]
95. Molavipordanjani, S.; Emami, S.; Mardanshahi, A.; Amiri, F.T.; Noaparast, Z.; Hosseinimehr, S.J. Novel ^{99m}Tc -2-arylimidazo[2,1-b]benzothiazole derivatives as SPECT imaging agents for amyloid- β plaques. *Eur. J. Med. Chem.* **2019**, *175*, 149–161. [[CrossRef](#)] [[PubMed](#)]
96. Sagnou, M.; Mavroidi, B.; Shegani, A.; Paravatou-Petsotas, M.; Raptopoulou, C.; Psycharis, V.; Pirmettis, I.; Papadopoulos, M.S.; Pelecanou, M. Remarkable Brain Penetration of Cyclopentadienyl $\text{M}(\text{CO})_3^+$ ($\text{M} = ^{99m}\text{Tc}$, Re) Derivatives of Benzothiazole and Benzimidazole Paves the Way for Their Application as Diagnostic, with Single-Photon-Emission Computed Tomography (SPECT), and Therapeutic Agents for Alzheimer's Disease. *J. Med. Chem.* **2019**, *62*, 2638–2650. [[PubMed](#)]

97. Jokar, S.; Behnammanesh, H.; Erfani, M.; Sharifzadeh, M.; Gholami, M.; Sabzevari, O.; Amini, M.; Geramifae, P.; Hajiramezanali, M.; Beiki, D. Synthesis, biological evaluation and preclinical study of a novel ^{99m}Tc -peptide: A targeting probe of amyloid- β plaques as a possible diagnostic agent for Alzheimer's disease. *Bioorg. Chem.* **2020**, *99*, 103857. [[CrossRef](#)]

Publisher's Note: MDPI stays neutral with regard to jurisdictional claims in published maps and institutional affiliations.



© 2020 by the authors. Licensee MDPI, Basel, Switzerland. This article is an open access article distributed under the terms and conditions of the Creative Commons Attribution (CC BY) license (<http://creativecommons.org/licenses/by/4.0/>).